
Redundancy parameterization and inverse kinematics of 7-DOF revolute manipulators

Alexander J. Elias and John T. Wen

Abstract

Seven degree-of-freedom (DOF) robot arms have one redundant DOF which does not change the motion of the end effector. The redundant DOF offers greater manipulability of the arm configuration to avoid obstacles and singularities, but it must be parameterized to fully specify the joint angles for a given end effector pose. For 7-DOF revolute (7R) manipulators, we introduce a new concept of generalized shoulder-elbow-wrist (SEW) angle, a generalization of the conventional SEW angle but with an arbitrary choice of the reference direction function. The SEW angle is widely used and easy for human operators to visualize as a rotation of the elbow about the shoulder-wrist line. Since other redundancy parameterizations including the conventional SEW angle encounter an algorithmic singularity along a line in the workspace, we introduce a special choice of the reference direction function called the stereographic SEW angle which has a singularity only along a half-line, which can be placed out of reach. We prove that such a singularity is unavoidable for any parameterization. We also include expressions for the SEW angle Jacobian along with singularity analysis. Finally, we provide efficient and singularity-robust inverse kinematics solutions for most known 7R manipulators using the general SEW angle and the subproblem decomposition method. These solutions are often closed-form but may sometimes involve a 1D or 2D search in the general case. Search-based solutions may be converted to finding zeros of a high-order polynomial. Inverse kinematics solutions, examples, and evaluations are available in a publicly accessible repository.

Keywords

Kinematics, Redundant Robots, Industrial Robots, Space Robotics and Automation, Telerobotics and Teleoperation, Humanoid Robot Systems

1 Introduction

Most industrial robot arms have six revolute joints to control the six degrees of freedom (DOF) of the robot end effector pose, but a human arm has seven DOF: three for the shoulder, one for the elbow, and three for the wrist. Similarly, there are 7-DOF revolute (7R) robot arms such as the Robotics Research Corporation (RRC) arm (Robotics Research Corporation 2005), Baxter (Rethink Robotics 2015), Sawyer (Rethink Robotics 2022), Yumi (ABB 2022), and the Space Station Robot Manipulator System (SSRMS) (Crane III, Duffy and Carnahan 1991). The extra *redundant* degree of freedom means that there is a continuum of arm configurations for a given hand or robot end effector pose. Holding the end effector pose constant while moving through the continuum of arm configurations, called self-motion, commonly looks like the elbow rotating around the line passing from the shoulder to the wrist (Figure 1). Benefits of 7R arms over 6R arms include using redundancy to avoid singularities and obstacles (Hollerbach

1985), optimize motion time (Chen, Zhang, Huang, Wu and Ota 2023), avoid joint motion limits (Flacco, De Luca and Khatib 2012), and avoid joint torque limits (Hollerbach and Suh 1987).

To fully specify the pose of a 7R robot up to a finite number of solutions, the end effector pose must be augmented by a secondary task. During pure self-motion, the only difference between parameterizations would be the rate of movement; differences between parameterizations are made clearer during motion of the end effector. Redundancy in human and many 7R robot arms may be conveniently parameterized by the shoulder-elbow-wrist (SEW) angle, sometimes called the elbow angle,

Department of Electrical, Computer, and Systems Engineering, Rensselaer Polytechnic Institute, Troy, NY

Corresponding author:

Alexander J. Elias, Rensselaer Polytechnic Institute, Troy, NY.
Email: eliasa3@rpi.edu

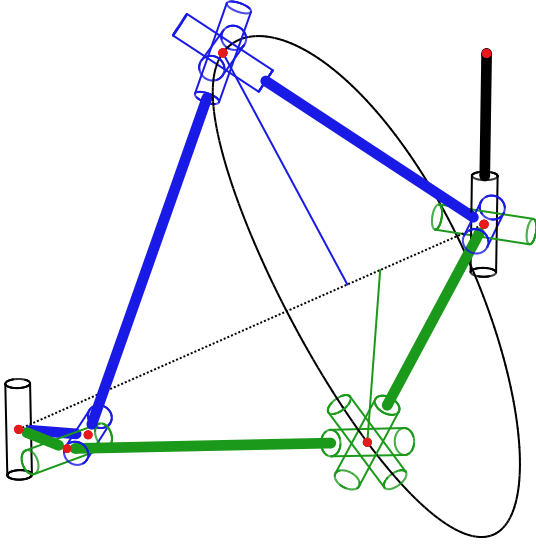


Figure 1. Self-motion for a Motoman SIA50D (R-R-3R^E-2R) robot arm. For a given end effector pose, the spherical elbow may be on a curve which is the intersection of a torus formed by joints 1 and 2 a sphere centered at joints 6 and 7.

which characterizes the rotation of the plane containing the shoulder, elbow, and wrist about the shoulder-wrist line with respect to a reference plane. This reference plane is conventionally chosen as the plane containing the shoulder-wrist line and a reference vector. This redundancy parameterization is easy to visualize and is widely used in applications such as space teleoperation (Tsumaki, Fiorini, Chalfant and Seraji 2001; Pryor 2023; Zhu, Wang and Ma 2021) partly because it is intuitive for space robot operators (Swaim, Arend, Bevill, Decker, Dunn, Read, Reiher, Richard, Ruta and Teplitz 1994). Furthermore, for certain 7R arms, the inverse kinematics has an analytical solution, i.e., for a given robot end effector pose and SEW angle, the finite set of the seven robot joint angles may be solved directly instead of iteratively. The augmented Jacobian, the 7×7 matrix that maps the joint velocity vector to the end effector spatial velocity and the SEW angular velocity, is easily characterized.

An issue with the conventional SEW angle becomes apparent when the shoulder-wrist line is collinear with the reference vector because the reference plane becomes undefined. This is referred to as an *algorithmic singularity*, a singularity due to the choice of redundancy parameterization. Algorithmic singularities are the main weakness of parameterizations like the SEW angle (Dupuis 2001) because robots experience undesirable behavior near them just as for kinematic singularities. For example, being near an algorithmic singularity may result in dangerously large elbow movement, which is especially problematic for teleoperation (Tsumaki, Fiorini, Chalfant and Seraji 2001).

It also leads to poor convergence for iterative algorithms as well as numerical precision problems since many significant digits are required to accurately specify the robot pose. Designers must carefully choose the reference direction to avoid singularities, but it is often inevitable to waste regions of the reachable workspace (Carignan and Howard 2000; Carignan, Lane and Churchill 2001; Naylor, Atkins and Roderick 2007; Scott and Carignan 2008).

In this paper, we introduce a new generalized concept of SEW angle which includes the conventional SEW angle as a special case. We show that an algorithmic singularity is unavoidable for any redundancy parameterization, but a special choice of the generalized SEW angle based on the stereographic projection changes the bidirectional singularity to a unidirectional singularity. The singularity direction may be located towards the base of the arm so it will not be encountered in the robot workspace. The advantages of the SEW angle redundancy parameterization are still retained for the generalized SEW angle, including analytical inverse kinematics for many 7R arms, intuitive teleoperation, and an analytical Jacobian. Most existing algorithms which use the conventional SEW angle or its Jacobian can be easily adapted to use the general SEW angle, including the stereographic SEW angle

We also provide inverse kinematics (IK) solutions using the general SEW angle for most 7R robots used in practice or mentioned in the literature including general 7R manipulators, as well as arms which do not yet exist. These solutions are built upon IK-Geo, an open-source and easy-to-use IK solver based on a unifying subproblem decomposition approach (Elias and Wen 2024). The solutions are often closed-form, but for some robots IK is solved using a 1D or 2D search over a compact set. These analytical and semi-analytical methods are efficient, precise, and stable, especially compared to Jacobian-based algorithms. They are also robust to singularities and find all IK solutions, including singular solution, rather than just one close to an initial guess. For branches without exact solutions, they return continuous non-exact and sometimes least-squares solutions. This allows Cartesian motion directly through singularities to switch between different IK branches without resorting to joint control. We also demonstrate converting a search-based solution to a polynomial solution: To the best of our knowledge, we are the first to provide a polynomial in the tangent half-angle of one joint which corresponds to IK solutions of a 7R robot parameterized by SEW angle.

We offer the following new contributions in this paper:

- We introduce the stereographic SEW angle, a new redundancy parameterization that encounters a singularity only along a half-line instead of a full line as in the conventional SEW angle. This

significantly enlarges of the singularity-free region of the workspace.

- We show that algorithmic singularities are unavoidable for any redundancy parameterization. We classify different types of singularities for 7R arms and discuss when singularities are concurrent.
- We efficiently solve IK for any 7R manipulator parameterized by the conventional or stereographic SEW angle using the subproblem decomposition approach. We categorize 7R robots based on intersecting or parallel axes and choices of shoulder, elbow, and wrist locations. We also demonstrate solving IK for a 7R manipulator parameterized by conventional or stereographic SEW angle by finding a high-order polynomial in the tangent half-angle of one joint.

The remainder of the paper is organized as follows. In Section 2 we discuss previous related works, and we describe forward kinematics for 7R arms using coordinate-free notation and the product of exponentials approach. We introduce the general SEW angle in Section 3 including forward and differential kinematics, we discuss singularity conditions, and we relate it to the conventional SEW angle. In Section 4 we prove the existence of algorithmic singularities for any redundancy parameterization. We define the stereographic SEW angle in Section 5, discuss its relationship to stereographic projection and its singularity behavior, and provide an example comparing using the conventional and stereographic SEW angle formulations. We provide IK solutions with examples in Section 6, and we conclude in Section 7.

Inverse kinematics solutions, examples, and evaluations are available in a publicly accessible repository*.

2 Background

2.1 Robot Notation

To notate different families of robot kinematic parameters, we follow and slightly extend the notation introduced by Pieper (1969). A single revolute joint is notated by R, and when multiple joints intersect, they may be notated as 2R or 3R for two or three intersecting joints, respectively. The joints are written in order from the base to the end effector. For example, a robot with a spherical shoulder, a revolute elbow, and a spherical wrist may be notated as 3R-R-3R. We also introduce the notation of 2R|| and 3R|| to indicate two or three consecutive parallel revolute joints. Note that since a given joint may intersect or be parallel with both the joint before it and the joint after it, a single robot may fall into multiple robot kinematic families.

We use superscript S, E, or W to indicate when the shoulder, elbow, or wrist is placed at a joint or joint intersection. For example, 2R^E would indicate a 2R joint

with the elbow placed at the joint intersection. Unless otherwise indicated, a robot has its shoulder on the first joint or joint intersection and has its wrist on its last joint or joint intersection.

2.2 Related Literature

The analysis and parameterization of the redundant degree of freedom in 7R manipulators has been primarily driven by space robotics applications and more recently motivated by industrial robots in manufacturing and humanoid robots. Early papers focused on analyzing the geometry, topology, and differential kinematics of 7-DOF manipulators. Baillieul (1985) introduced the concept of the augmented Jacobian (termed the extended Jacobian) and discussed the algorithmic singularity. Hollerbach (1985) discussed options for 7-DOF manipulator designs, including how adding an extra degree of freedom removes internal singularities. The paper discusses the self-motion manifold and was one of the earliest papers to recommend using the conventional SEW angle (with the reference vector pointing up). Burdick and Seraji (1989) gave an overview of the topology of the self-motion manifold. Kreutz-Delgado, Long and Seraji (1990, 1992) provided a detailed analysis of the conventional SEW angle with application to 3R-R-3R arms and the RRC arm, which has no intersecting consecutive joint axes. They also provided the expression for the SEW Jacobian and singularity analysis.

Parameterizing the redundant degree of freedom is not strictly necessary to control a 7R arm. For example, one can use resolved velocity or resolved acceleration control using the weighted or unweighted Jacobian pseudoinverse, or perform optimization of some other task which is not a function of joint angles. A critical problem with these controllers is non-cyclicity (Swaim, Arend, Bevil, Decker, Dunn, Read, Reiher, Richard, Ruta and Teplitz 1994; Stanczyk, Peer and Buss 2006). These controllers are non-conservative, so if the robot makes a closed loop in its end effector path, the elbow may not return to its original position. This is unacceptable in any industrial or mission-critical scenario. Furthermore, these differential redundancy resolution techniques have stability problems: Minimizing joint velocity, joint torque, or joint acceleration locally does not prevent the robot from approaching a singularity (Baillieul, Hollerbach, Brockett, Martin, Percy and Thomas 1987; Hollerbach and Suh 1987). Extra work must be done to stabilize such a controller to prevent it from driving itself into a singularity (O'Neil and Chen 2000).

On the other hand, augmenting the task space with a function of the joint angles, such as the SEW angle, ensures

*<https://github.com/rpiRobotics/stereo-sew>

cyclical behavior and gives direct control of the redundant degree of freedom over the entire trajectory (Seraji 1989). By using a global rather than local approach, task-space behavior is immediately known without using IK. This leads to intuitive teleoperation and programming and allows for transferring task-space behavior between robots or even between humans and robots (Stanczyk, Peer and Buss 2006; Lamperti, Zanchettin and Rocco 2015).

It is no wonder that SEW angle is widely used for teleoperation in space (Tsumaki, Fiorini, Chalfant and Seraji 2001; Zhu, Wang and Ma 2021; Pryor 2023), underwater (Carignan and Howard 2000; Carignan, Lane and Churchill 2001; Naylor, Atkins and Roderick 2007; Scott and Carignan 2008), and in surgery (Su, Sandoval, Makhdoomi, Ferrigno and De Momi 2018b; Su, Sandoval, Vieyres, Poisson, Ferrigno and De Momi 2018c; Su, Yang, Ferrigno and De Momi 2019).

The SEW angle allows for ease of global planning (Pryor 2023) since the entire solution space can be considered, and it can be easily extended to incorporate hybrid force-motion or impedance control of both end effector motion and self-motion (Su, Yang, Ferrigno and De Momi 2019; Su, Sandoval, Makhdoomi, Ferrigno and De Momi 2018b; Su, Sandoval, Vieyres, Poisson, Ferrigno and De Momi 2018c; Xiong, Zhou and Yao 2020).

Additionally, the SEW angle is compatible with other optimizations to avoid obstacles, joint angle limits, joint torque limits, or singularities, or to maximize metrics like force transmission ratio (Carignan and Howard 2000; Carignan, Lane and Churchill 2001; Naylor, Atkins and Roderick 2007; Scott and Carignan 2008; Stanczyk and Buss 2004; Lee and Buss 2006; Su, Yang, Ferrigno and De Momi 2019; Su, Sandoval, Makhdoomi, Ferrigno and De Momi 2018b; Su, Sandoval, Vieyres, Poisson, Ferrigno and De Momi 2018c).

There are also applications of the SEW angle not just to typical 7-DOF robots, but also to human arms and wearable robots (Kim, Miller, Al-Refai, Brand and Rosen 2011; Kim, Miller, Byl, Abrams and Rosen 2012; Li, Roldan, Milutinović and Rosen 2013; Wang and Artemiadis 2013; Liu, Chen and Steil 2017; Su, Enayati, Vantadori, Spinoglio, Ferrigno and De Momi 2018a; Wang, Peng, Hou, Li, Luo, Chen and Wang 2019; Li, Han, He, Li, Liu and Xiong 2022).

There have been several other proposed redundancy parameterizations besides the conventional SEW angle. Yan, Mu and Xu (2014) attempted to address the singularity issue of the conventional SEW angle by proposing a method which picks two different reference vectors and switches between the corresponding SEW angles when one of them encounters a singularity. The resulting parameterization is non-smooth, and singularities would still be present. Furthermore, this parameterization is no longer a function

of the joint angles and will therefore be noncyclical. Similar issues occur for any other method which switches between parameterizations, such as the method proposed by An, Clement and Reed (2014) to switch between the SEW angle and the first joint angle. Shimizu, Yoon and Kitagaki (2007) used the SEW angle where the reference plane is formed by the elbow when joint three is zero. They explained the reference plane is undefined in a shoulder or elbow singularity, so there is no benefit in terms of singularity existence as compared to the conventional SEW angle. One can also parameterize the redundant DOF by choosing one joint angle and reducing the problem to the IK of a non-redundant 6R manipulator, but this introduces singularities resulting from the equivalent 6R robot. In fact, it appears that all proposed redundancy parameterizations up to now have a bidirectional singularity. This makes the stereographic SEW angle the only parameterization proposed so far with a unidirectional singularity structure.

Numerous authors have found the IK solutions of 7R arms parameterized by one joint angle. Xu, She and Xu (2014) found the inverse kinematics for a 2R-3R||-2R arm by parameterizing the redundant degree of freedom with any joint angle. Jiang, Huo, Liu and Liu (2013) found the R-R-3R-2R arm IK solution by parameterizing joint 1. An, Clement and Reed (2014) found the IK solution for a 2R-2R-3R arm by parameterizing joint 1. Tondu (2006) found IK for a 3R-R-3R arm by parameterizing joint 1, and Pfullner (2016) found the IK for a 3R-R-3R arm by parameterizing joint 2 or 3. Nammoto and Kosuge (2012) found the IK solutions for an R-R-3R-2R arm parameterized by joint 1. Sinha and Chakraborty (2019) found a 1D search-based IK for R-2R-2R-2R arms parameterized by joint 1.

Many papers provide inverse kinematics solutions using the conventional SEW angle. Gong, Li and Zhang (2019); Tian, Xu and Zhan (2021); Faria, Ferreira, Erlhagen, Monteiro and Bicho (2018) used the conventional SEW angle to provide closed-form IK for 3R-R-3R arms. An, Clement and Reed (2014) found a closed-form IK solution for 2R-2R-3R arms. Many papers used an iterative IK method with an approximate closed-form solution as a starting point: Wang, Zhao, Wang, Zhang, Li and Liu (2021) for an R-2R-R-3R arm, and Ma, Xie, Jiang and Liu (2021) for a 2R-3R||-2R arm. (Zhao, Yang, Zhao, Yang and Zhao 2023) also found an iterative solution for an 2R-3R||-2R. The paper states closed-form IK is not possible when using SEW angle. However, (Jin, Liu, Wang and Liu 2020) solved IK for a 2R-3R||-2R manipulator in closed form by defining the SEW plane to be perpendicular to joint axes 3, 4, and 5. Until now, no one has proposed a unified method of inverse kinematics for any 7R manipulator parameterized by SEW angle which does not rely on the Jacobian.

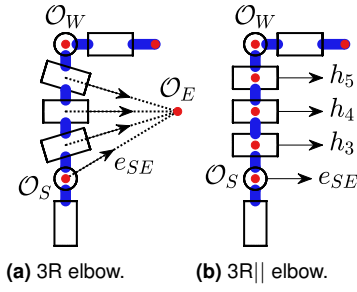


Figure 3. A 3R|| joint is the limit of a 3R joint as the intersection point moves to infinity. If this joint is the elbow, then although in the limit p_{SE} has infinite length, the normalized vector e_{SE} is defined and is equal to the three parallel joint axes.

\vec{p}_{SW} and \vec{p}_{SE} represented in \mathcal{E}_0 . The shoulder-wrist vector is

$$p_{SW} = p_{0T} - R_{07}p_{7T} + R_{07}p_{7W} - p_{0S}, \quad (4)$$

and the shoulder-elbow vector is

$$p_{SE} = p_{01} + R_{01}p_{12} + R_{02}p_{23} + R_{03}p_{3E} - p_{0S}. \quad (5)$$

It is often helpful for the inverse kinematics solution to set the shoulder, elbow, or wrist offset vector to 0 so that \mathcal{O}_S , \mathcal{O}_E , or \mathcal{O}_W is coincident with the link frame origin.

On some robots, such as those with three consecutive parallel axes, it may be helpful to define the shoulder-elbow vector p_{SE} to be a unit vector e_{SE} which is equal to one of the joint axes represented in the base frame. For example, we may pick $p_{SE} = e_{SE} = R_{02}h_3$. Since three parallel joint axes are the limit of three intersecting axes where the point of intersection moves infinitely far away, this can be interpreted as choosing p_{SE} to be the normalized vector pointing at this intersection (Figure 3). For some robots this leads to closed-form inverse kinematics using the subproblem decomposition approach.

3 General SEW Angle

3.1 Kinematics Description

Consider a 7-DOF arm with shoulder, elbow, and wrist defined. The SEW (shoulder-elbow-wrist) angle ψ , also commonly referred to as the arm angle or swivel angle, is the angle of the shoulder-elbow vector p_{SE} about the shoulder-wrist vector p_{SW} with respect to some reference vector. Consider an arbitrary mapping, called the reference direction function, from the shoulder-wrist vector p_{SW} to a unit vector e_x that is orthogonal to p_{SW} . Denote this mapping by $e_x = f_x(p_{SW})$. From this we can form an orthonormal basis (e_x, e_y, e_{SW}) , where e_{SW} is the normalized p_{SW} and $e_y = e_{SW}^\times e_x$. This frame may be used to measure the SEW angle.

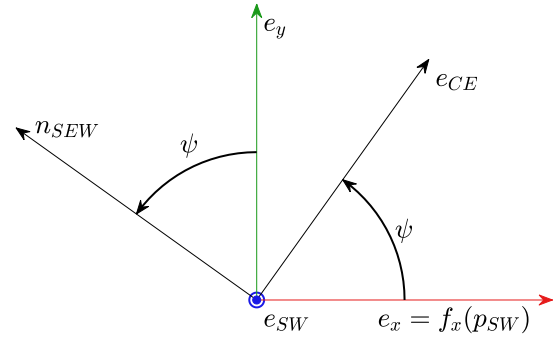
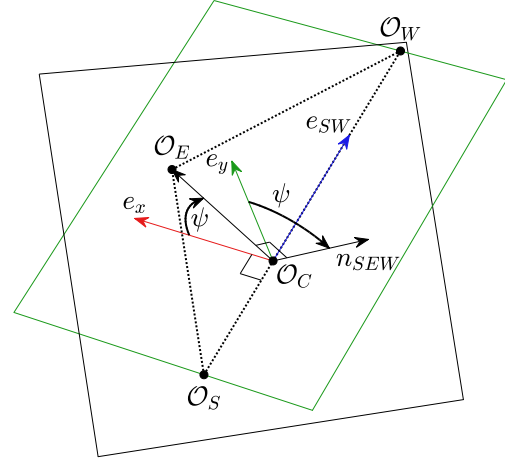


Figure 4. The SEW angle ψ is the angle of the elbow measured from $e_x = f_x(p_{SW})$ about e_{SW} , which is also the angle of the SEW plane normal vector n_{SEW} measured from e_y about e_{SW} . In the general SEW angle, the reference direction function $f_x(p_{SW})$ is arbitrary but with the constraints that the output is unit length and orthogonal to p_{SW} .

There are two equivalent definitions of the SEW angle, as shown in Figure 4. The elbow definition is that ψ is the angle between shoulder-elbow vector p_{SE} and reference vector e_x measured along the shoulder-wrist rotational axis e_{SW} . The plane definition is that ψ is the angle between n_{SEW} , which is the normal vector of the SEW plane containing the shoulder, elbow and, wrist, and e_y , which is the normal vector of the reference plane containing the shoulder, wrist, and reference vector e_x . While the elbow definition is helpful for forward kinematics, the plane definition is more useful for inverse kinematics when using the subproblem decomposition approach.

Using the elbow definition, the SEW angle is

$$\psi = \arg \min_{\theta} \|\mathbb{R}(e_{SW}, \theta)e_x - p_{SE}\|. \quad (6)$$

We can also rewrite this more compactly by removing the component of p_{SE} along e_{SW} . Let \mathcal{O}_C be the point on p_{SW} such that p_{CE} is orthogonal to e_{SW} , i.e.,

$$p_{CE} = -e_{SW}^\times p_{SE}. \quad (7)$$

Then,

$$e_{CE} = R(e_{SW}, \psi)e_x, \quad (8)$$

where $e_{CE} = p_{CE} / \|p_{CE}\|$.

Using the plane definition, the SEW angle is

$$n_{SEW} = R(e_{SW}, \psi)e_y, \quad (9)$$

where the normal of the plane containing the shoulder, elbow, and wrist is

$$n_{SEW} = \frac{k_{SEW}}{\|k_{SEW}\|}, \quad (10a)$$

$$k_{SEW} = p_{SW}^\times p_{SE}. \quad (10b)$$

Subproblem 1 (Elias and Wen 2024) may be used to solve the forward kinematics for the SEW angle, which is

$$\psi = \text{atan2}(e_y^T p_{SE}, e_x^T p_{SE}) \quad (11a)$$

$$= \text{atan2}(e_y^T p_{CE}, e_x^T p_{CE}) \quad (11b)$$

$$= \text{atan2}(-e_x^T n_{SEW}, e_y^T n_{SEW}) \quad (11c)$$

$$= \text{atan2}(-e_x^T k_{SEW}, e_y^T k_{SEW}). \quad (11d)$$

To perform inverse kinematics, we can use a given (R_{0T}, p_{0T}) to find p_{SW} from (4). Next, use the reference direction function $f_x(p_{SW})$ to find e_x or e_y . Then, for a given ψ , we can calculate e_{CE} or n_{SEW} using (8) or (9), respectively, which may then be used to determine the joint angle vector q . For the subproblem decomposition approach in Section 6, we always calculate n_{SEW} .

Some robots are not easily parameterized using the SEW angle. For example, the FANUC R-1000iA/120F-7B is an R-3R||-3R robot (FANUC 2022). The redundant degree of freedom in this family of robots is the movement of joints 2, 3, and 4, along with the corresponding movement in the spherical wrist, which results in the shortening or lengthening of the distance between joints 2 and 4 (Shi, Guo, Chen, Chen and Yang 2021). However, with \mathcal{O}_S placed at joint 1 and \mathcal{O}_W placed at the spherical wrist, there is no movement of joints 2, 3, or 4 around e_{SW} during self-motion; they stay in the same half plane and the SEW angle would fail to parameterize the redundant degree of freedom. Robots such as this are better parameterized by specifying a joint angle. (A good choice for this robot is q_3 .)

To find the Jacobian of the SEW angle with respect to the joint angles, J_ψ , we will write it in terms of the partial Jacobians mapping joint angular velocities to the linear velocity of \mathcal{O}_E and \mathcal{O}_W :

$$\dot{p}_{SE} = \dot{p}_{0E} = J_E \dot{q}, \quad \dot{p}_{SW} = \dot{p}_{0W} = J_W \dot{q} \quad (12)$$

If \mathcal{O}_S is not constant in the base frame, then J_S is nonzero and we must subtract $J_S \dot{q}$.

Taking the total derivative of (11b), we obtain

$$\dot{\psi} = \frac{1}{\|p_{CE}\|} (e_{SW}^\times e_{CE})^T \dot{p}_{CE} - e_y^T \dot{e}_x. \quad (13)$$

Geometrically, these two terms are the angular velocities of p_{CE} and e_x around the axis of rotation e_{SW} . Define J_{f_x} such that $\dot{e}_x = J_{f_x} \dot{p}_{SW}$, which depends on the choice for the function $f_x(p_{SW})$. Then by using (7), we can expand (13) as

$$\dot{\psi} = \frac{1}{\|p_{CE}\|} (e_{SW}^\times e_{CE})^T \dot{p}_{0E} - \left(e_y^T J_{f_x} + \frac{e_{SW}^T p_{SE}}{\|p_{SW}\| \|p_{CE}\|} (e_{SW}^\times e_{CE})^T \right) \dot{p}_{0W} \quad (14)$$

Since we have

$$\dot{\psi} = J_\psi \dot{q} \quad (15)$$

we can write the SEW Jacobian as

$$J_\psi = J_{\psi,E} J_E + J_{\psi,W} J_W, \quad (16)$$

where

$$J_{\psi,E} = \frac{(e_{SW}^\times e_{CE})^T}{\|p_{CE}\|}, \quad (17)$$

$$J_{\psi,W} = -e_y^T J_{f_x} - \frac{e_{SW}^T p_{SE}}{\|p_{SW}\| \|p_{CE}\|} (e_{SW}^\times e_{CE})^T. \quad (18)$$

We can form the 7×7 augmented Jacobian J_A by stacking J and J_ψ :

$$J_A = \begin{bmatrix} J \\ J_\psi \end{bmatrix}, \quad \begin{bmatrix} \omega \\ v \\ \dot{\psi} \end{bmatrix} = J_A \dot{q}. \quad (19)$$

The augmented task space, which has the end effector orientation as well as the SEW angle, has 7 degrees of freedom.

3.2 Singularity Conditions

When controlling a robot using end effector pose augmented with SEW angle, singularities occur when the matrix J_A^{-1} does not exist. When a robot is close to a singularity, there may be large internal joint motion which is undesirable and possibly dangerous, as well as issues with iterative algorithm convergence and numerical precision. There are a number of conditions which result in a singularity, as shown in Table 2. Multiple singularity types can occur simultaneously.

The self-motion manifold for 7-DOF spatial manipulators is a curve in joint space for which all points map to the same end effector pose (Burdick and Seraji 1989). A single end effector pose may have multiple self-motion manifolds, where each manifold belongs to a different inverse kinematics branch. This manifold exists independently of any

Table 2. Singularity conditions. Cases 2 and 3 are both algorithmic singularities.

Condition	Singularity Name	Description
1. J loses rank	Kinematic	End effector cannot move in one direction
A. Null space of J tangent to self-motion manifold	Internal	Extra continuous self-motion possible
B. Null space of J not tangent to self-motion manifold	Boundary	Self-motion is instantaneous
2. J_A singular (Full rank J and J_ψ)	Augmentation	Self-motion doesn't change SEW angle
3. J_ψ undefined	SEW Angle	SEW angle undefined
A. $\mathcal{O}_S, \mathcal{O}_E, \mathcal{O}_W$ collinear	Collinear	Depends on choice of $\mathcal{O}_S, \mathcal{O}_E, \mathcal{O}_W$
B. J_{f_x} undefined	Coordinate	Depends on choice of $f_x(p_{SW})$

parameterization of the redundant degree of freedom, and the goal of parameterizations such as SEW angle is to assign a value to each point on the self-motion manifold. When J is full rank, the self-motion manifold is one-dimensional and the null space of J is the tangent to the self-motion manifold.

A kinematic singularity occurs when J loses rank, meaning some spatial velocity of the end effector cannot be achieved. This is a condition that depends on the kinematics and joint angles of the robot and does not depend on the parameterization of the redundant degree of freedom. There are two types of kinematic singularities: Internal singularities and boundary singularities. At internal singularities, e.g., when two joint axes are collinear, the null space of J is tangent to the self-motion manifold. A new degree of freedom for self-motion is introduced, but parameterizations such as the SEW angle may not be able to parameterize this degree of freedom. At boundary singularities, e.g., when two links are collinear, the null space of J is not tangent to the self-motion manifold, and self-motion is only instantaneous. In some cases, the entire null space of J causes only instantaneous rather than continuous self-motion, and the self-motion manifold degenerates into a point: The self-motion manifold is zero-dimensional and any parameterization for the redundant degree of freedom is unnecessary because for each inverse kinematics branch there is only one choice for ψ .

For all conditions other than the kinematic singularity, we call them algorithmic singularities as they occur not because of the robot itself but because of the algorithms we use to parameterize the redundancy. Many authors (Kreutz-Delgado, Long and Seraji 1990; Chiaverini 1997; Marani, Kim, Yuh and Chung 2003) have defined algorithmic singularities to occur when J_A^{-1} does not exist and J and J_ψ are separately full rank. However, as in Wang and Kazerounian (1995); Faria, Ferreira, Erlhagen, Monteiro and Bicho (2018), we generalize the definition of algorithmic singularity to include cases where J_ψ may not be full rank (i.e., may be a zero vector) or may not exist.

One type of algorithmic singularity is when J_A loses rank, which is possible even when J and J_ψ are full rank. We call this the augmentation singularity, as it occurs only when end effector and SEW angle rates are considered

simultaneously. Algebraically, this singularity occurs when J_ψ is linearly dependent with the rows of J . Geometrically, this means self-motion does not cause a change in SEW angle.

The second type of algorithmic singularity is when J_A^{-1} does not exist because J_ψ does not exist, which we call the SEW angle singularity. There are two cases for the SEW angle singularity. The first case, called the collinear singularity, happens when $\mathcal{O}_S, \mathcal{O}_E,$ and \mathcal{O}_W are collinear, which causes $p_{SW} = 0$ or $p_{CE} = 0$. The second case, called the coordinate singularity, is when J_ψ does not exist because J_{f_x} does not exist. In fact, in Section 4, we show that for any choice of $f_x(p_{SW})$ there will always be choices of p_{SW} that causes singularities in J_{f_x} .

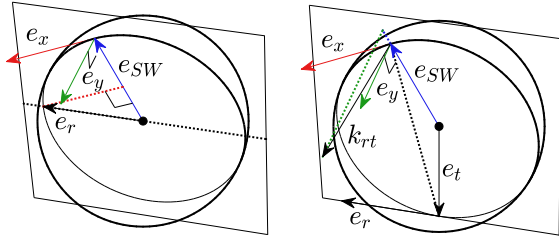
Given that the collinear singularity is unavoidable for some robots, it can be beneficial to place $\mathcal{O}_S, \mathcal{O}_E,$ and \mathcal{O}_W such that the SEW angle is undefined exactly when there is only one choice for elbow position per IK branch due to boundary singularities. This reduces the total number of singularities in the workspace. In the case of a 2R-2R-3R robot, placing the shoulder, elbow, and wrist at the joint intersections means that SEW angle is undefined when the robot has no self-motion of the elbow to parameterize anyway.

The condition of J_ψ losing rank, meaning $J_\psi = 0$, may occur for a general parameterization of the redundant degree of freedom, but for most reasonable choices of placement of $\mathcal{O}_S, \mathcal{O}_E,$ and \mathcal{O}_W , this condition will not occur for the SEW angle. Choi, Oh, Oh, Park and Chung (2004) called this case the secondary task singularity.

3.3 Conventional SEW Angle

The conventional SEW angle, shown in Figure 5(a), is a widely used parameterization. Kreutz-Delgado, Long and Seraji (1990) were the first to provide detailed analysis of the conventional SEW angle, but the idea was described earlier by Hollerbach (1985).

Let e_r be an arbitrary unit reference vector. For the conventional SEW angle, we define the reference direction



(a) Conventional SEW angle. (b) Stereographic SEW angle.

Figure 5. Geometric interpretations for $e_x = f_x(p_{SW})$. (a) In the conventional SEW angle, e_x is the normalized version of the component of e_r orthogonal to e_{SW} , and e_y is normal to the plane containing e_{SW} and e_r . (b) In the stereographic SEW angle, k_{rt} is normal to the plane containing $e_{SW} - e_t$ and e_r , e_y is the normalized version of the component of k_{rt} orthogonal to e_{SW} , and e_x is normal to k_{rt} and e_{SW} .

function f_x as

$$e_x = f_x(p_{SW}) = e_y^\times e_{SW}, \quad (20a)$$

$$e_y = \frac{k_y}{\|k_y\|}, \quad (20b)$$

$$k_y = p_{SW}^\times e_r. \quad (20c)$$

Equivalently, $e_x = f_x(p_{SW})$ is the normalized $-e_{SW}^\times e_r$, so e_x is the unit vector orthogonal to e_{SW} closest to e_r .

The conventional SEW angle is intuitive to understand. $\psi = 0$ corresponds to e_{CE} pointing as much towards e_r as possible. This is similar to navigating on a globe using cardinal directions where e_r provides the north direction and the SEW angle is measured from north.

The conventional SEW angle becomes undefined and a coordinate singularity occurs when $k_y = p_{SW}^\times e_r = 0$, which occurs when p_{SW} is collinear with e_r . In this case, all possible choices of e_{CE} are equally close to e_r . This is akin to being on the north or south pole of a globe where there is no north direction and cardinal directions are undefined. If the shoulder is constant in the base frame, then this singularity occurs when the wrist is on the line spanned by e_r passing through the wrist, as shown in Figure 6(a).

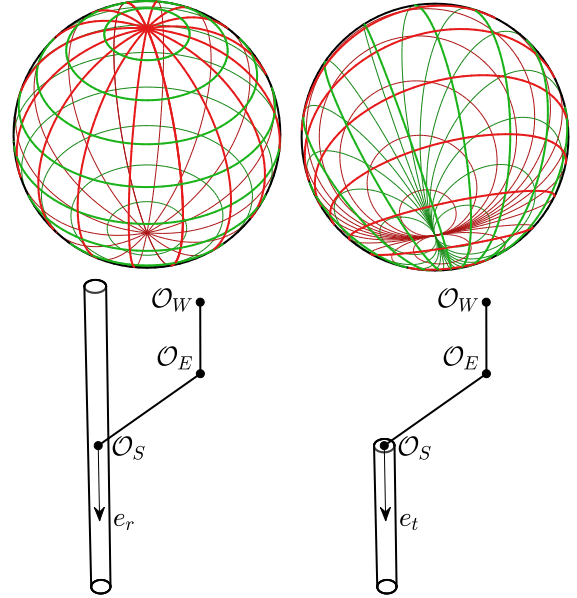
Using the elbow definition of the SEW angle, the conventional SEW angle can be succinctly expressed as

$$\psi = \arg \min_{\theta} \|\mathbb{R}(e_{SW}, \theta)e_r - p_{SE}\|, \quad (21)$$

(notice we may use e_r in place of e_x), which may be directly solved using Subproblem 1 as

$$\psi = \text{atan2}\left((e_{SW}^\times e_r)^T p_{SE}, -(e_{SW}^\times e_r)^T p_{SE}\right) \quad (22a)$$

$$= \text{atan2}(e_{SW}^T e_r^\times p_{CE}, e_r^T p_{CE}). \quad (22b)$$



(a) Conventional SEW angle. (b) Stereographic SEW angle.

Figure 6. Grid representing (e_x, e_y) for any choice of e_{SW} (top), and cylinder representing locations for O_W where the robot is at or near a coordinate singularity. (a) The conventional SEW angle has two singularities of order one, and the coordinate axes are lines of latitude and longitude. This results in a bidirectional singularity region in task space. (b) The stereographic SEW angle has a single singularity of order 2, which results in a unidirectional singularity region.

Alternatively, using the plane definition we have

$$\psi = \arg \min_{\theta} \|\mathbb{R}(e_{SW}, \theta)k_y - k_{SEW}\| \quad (23a)$$

$$= \text{atan2}((e_{SW}^\times k_y)^T k_{SEW}, -(e_{SW}^\times k_y)^T k_{SEW}) \quad (23b)$$

$$= \text{atan2}(e_{SW}^T k_y^\times k_{SEW}, k_y^T k_{SEW}). \quad (23c)$$

To calculate the Jacobian, we can express $-e_y^T \dot{e}_x$ as

$$\frac{e_x^T}{\|k_y\|} \dot{k}_y = \frac{e_x^T}{\|k_y\|} e_r^\times \dot{p}_{SW} = \frac{e_{SW}^T e_r}{\|k_y\|} e_y^T \dot{p}_{SW}. \quad (24)$$

Therefore, the Jacobian with respect to the wrist is

$$J_{\psi, W} = \frac{e_{SW}^T e_r}{\|k_y\|} e_y^T - \frac{e_{SW}^T p_{SE}}{\|p_{SW}\| \|p_{CE}\|} (e_{SW}^\times e_{CE})^T. \quad (25)$$

The Jacobian becomes undefined when $k_y = p_{SW}^\times e_r = 0$, again exhibiting the algorithmic singularity condition when e_r and p_{SW} become collinear.

4 Existence of Singularity

Hollerbach (1985) showed any revolute manipulator will have internal singularities associated with end effector orientation because it is always possible to find a pose with all joints lying in the same plane. Gottlieb (1986) used topology to arrive at the same conclusion: Every smooth map $T^n \rightarrow SO(3)$ must have singularities. Furthermore, he showed it is impossible to construct a smooth left-inverse of a mapping $T^4 \rightarrow SO(3)$, so there is no singularity-free function to map from orientation to joint angles in a 4R joint. (However, it is possible to always find joint angles to follow a given trajectory while avoiding singularities, but this does not follow a function and so will not be cyclical.)

In this section, we will show for a 7-DOF revolute arm with a sufficiently large workspace, e.g., a 3R-R-3R robot with orthogonal consecutive joints, and a task space augmented by any parameterization of the redundant degree of freedom, e.g., the SEW angle, there will always be an algorithmic singularity.

The so-called Hairy Ball Theorem (McGrath 2016) states that a continuous vector field on a sphere must have at least one point where it vanishes. We will use this theorem to show that a singularity must exist for any redundancy parameterization, $\phi : T^7 \rightarrow \mathbb{R}$. Given any end effector pose (R_{0T}, p_{0T}) and ϕ , there exists a finite number of inverse kinematics solutions q . Consider the sphere generated by a constant shoulder-wrist distance $\|p_{SW}\|$ such that the elbow \mathcal{O}_E does not lie on the shoulder-wrist line, i.e., p_{SE} and p_{SW} are not collinear. For any point on the sphere and a constant orientation and ϕ , find the inverse kinematics solution q that is on the same branch of the finite number of solutions. Define the vector field $e_{CE}(p_{SE})$ as the unit vector perpendicular to p_{SE} and pointing towards the elbow, which is the normalized version of $-e_{SW}^{\times 2} p_{SE}$, as shown in Figure 7. By the Hairy Ball Theorem, e_{CE} cannot be continuous everywhere on the sphere. This implies there is discontinuity in the joint angle while the wrist travels along the sphere, corresponding to the algorithmic singularity.

It is also straightforward to demonstrate that for the general SEW angle specifically, any choice of $f_x(p_{SW})$ must have a singularity. If we restrict the input to have some constant nonzero $\|p_{SW}\|$, then f_x defines a unit-magnitude vector field on a sphere. By the Hairy Ball Theorem, this vector field must be discontinuous. For the conventional SEW angle, the singularity occurs when $e_{SW} = \pm e_r$. If we choose ϕ to be the arm angle where e_x corresponds to e_{CE} when $q_3 = 0$ and the robot has a spherical wrist, then the singularity occurs when $e_{SW} = \pm h_1$.

Another common parameterization choice is $\phi(q) = q_1$. In this case if the robot has a spherical wrist then the singularity occurs when $e_{SW} = \pm R_{01} h_2$.

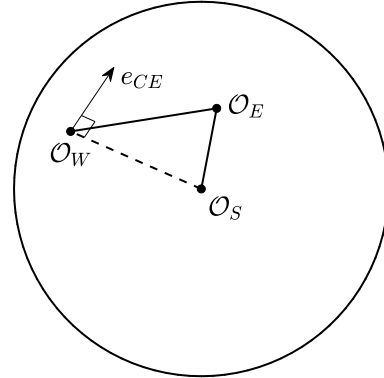


Figure 7. For each possible position of the wrist on a sphere around the shoulder while fixing the value of the arbitrary redundancy parameterization ϕ , define a unit vector tangent to the sphere and pointing towards the elbow. By Hairy Ball Theorem, this vector field cannot be continuous.

The Poincaré–Hopf theorem (Poincaré 1885; Hopf 1927) implies that not only must there be a singularity on the sphere, but the total order of singularities must be two. For this vector field, the order of the singularity is how many times the elbow rotates about the shoulder-wrist line as the wrist travels around the singularity once. In all the examples of ϕ shown above, there are two antipodal singularities of order one.

The goal of Section 5 is to find a redundancy parameterization that has a single singularity on this sphere of order two. This is in some sense the best-case singularity structure, as this results in a singularity along a half-line in the robot workspace. For most robots, this line can be chosen so that it goes into the structure holding the robot in place, meaning the singularity is out of the reachable workspace.

5 Stereographic SEW Angle

5.1 Definition

The conventional definition of the SEW angle in Section 3.3 encounters a singularity when the shoulder-wrist vector p_{SW} becomes collinear with the reference vector e_r . As discussed in Section 4, an algorithmic singularity is unavoidable, but we can reduce its impact by slightly changing the SEW angle definition so that the bidirectional line condition becomes a unidirectional half-line condition, as shown in Figure 6b.

For the stereographic SEW angle (Figure 5b), we define the reference direction function f_x as

$$e_x = f_x(p_{SW}) = \frac{k_x}{\|k_x\|}, \quad (26a)$$

$$k_x = k_{rt}^\times p_{SW}, \quad (26b)$$

$$k_{rt} = (e_{SW} - e_t)^\times e_r. \quad (26c)$$

This also means e_y is the normalized version of $-e_{SW}^\times k_{rt}$. e_t is an arbitrary vector chosen to place the singularity structure. We will show we need the conditions $\|e_r\| = 1$, $\|e_t\| = 1$, and $e_r^T e_t = 1$ to achieve the half-line singularity condition. If we instead set $e_t = 0$ then (26) becomes the conventional SEW angle definition.

Using the plane definition, the stereographic SEW angle can be written as

$$\psi = \arg \min_{\theta} \|\mathbb{R}(e_{SW}, \theta) k_{rt} - k_{SEW}\|, \quad (27)$$

which may be solved using

$$\psi = \text{atan2}(e_{SW}^T k_{rt}^\times k_{SEW}, k_{SEW}^T k_{rt}). \quad (28)$$

Using the elbow definition, we may equivalently write

$$\psi = \text{atan2}(k_{rt}^T p_{CE}, -e_{SW}^T k_{rt}^\times p_{CE}). \quad (29)$$

For any (e_r, e_t) with nonzero e_r we can always pick a new $(\tilde{e}_r, \tilde{e}_t)$ such that $e_r^T e_t = 1$ and $\|e_r\| = 1$ where the direction of k_{rt} is identical according to

$$\tilde{e}_r = \frac{e_r}{\|e_r\|}, \quad \tilde{e}_t = -\tilde{e}_r^\times e_t. \quad (30)$$

We can show that once we require $\|e_r\| = 1$ and $e_r^T e_t = 0$ (without loss of generality), the half-line singularity condition occurs if and only if $\|e_t\| = 1$. The algorithmic singularity corresponds to $k_x = 0$, which occurs when k_{rt} is a zero vector or collinear with e_{SW} . We consider two cases below:

1. $\|e_t\| \leq 1$: For two choices of e_{SW} , $k_{rt} = 0$:

$$e_{SW} = e_t \pm \sqrt{1 - \|e_t\|^2} e_r \quad (31)$$

This corresponds to the points on the unit sphere which intersect with the line spanned by e_r and translated by e_t .

2. $\|e_t\| \geq 1$: For two choices of e_{SW} , k_{rt} is collinear with e_{SW} :

$$e_{SW} = \frac{e_t}{\|e_t\|^2} \pm \sqrt{\|e_t\|^2 - 1} \frac{e_t^\times e_r}{\|e_t\|^2}. \quad (32)$$

This corresponds to the points on the unit sphere which is tangent to a plane passing through the line spanned by e_r and translated by e_t .

There are two unique singularities if $\|e_t\| < 1$ and 2 unique singularities if $\|e_t\| > 1$. By choosing $\|e_t\| = 1$, both (31) and (32) simplify to the half-line condition $e_{SW} = e_t$. Geometrically, this is because the line spanned by e_r and translated by e_t only passes through one point on the unit sphere (at e_t), and the only plane tangent to the unit sphere and passing through the line spanned by e_r and translated by e_t is tangent at e_t . If we instead set $e_t = 0$, then we recover the conventional SEW angle.

A good choice of e_t is to point in the opposite direction of the robot workspace (e.g., into the ground) so that the singularity will not affect the robot operation.

For the Jacobian, we must calculate

$$-e_y^T \dot{e}_x = -\frac{1}{\|k_x\|} e_y^T \dot{k}_x. \quad (33)$$

Recall that $k_x = k_{rt}^\times p_{SW}$, which means the derivative is

$$\dot{k}_x = k_{rt}^\times \dot{p}_{SW} - p_{SW}^\times \dot{k}_{rt}, \quad (34)$$

and so

$$-e_y^T \dot{e}_x = -\frac{(e_y^\times k_{rt})^T}{\|k_x\|} \dot{p}_{SW} + \frac{(e_y^\times p_{SW})^T}{\|k_x\|} \dot{k}_{rt}. \quad (35)$$

We can rewrite the first term as

$$\begin{aligned} -\frac{(e_y^\times k_{rt})^T}{\|k_x\|} \dot{p}_{SW} &= -\frac{e_{SW}^T k_{rt}}{\|k_x\|} e_x^T J^W \dot{q} \\ &= \frac{e_{SW}^T e_t^\times e_r}{\|k_x\|} e_x^T J^W \dot{q}. \end{aligned} \quad (36)$$

Notice that

$$\dot{e}_{SW} = -\frac{e_{SW}^\times}{\|p_{SW}\|} \dot{p}_{SW}. \quad (37)$$

The second term can be written as

$$\begin{aligned} \frac{(e_y^\times p_{SW})^T}{\|k_x\|} \dot{k}_{rt} &= \frac{\|p_{SW}\|}{\|k_x\|} e_x^T \left(e_r^\times \frac{e_{SW}^\times}{\|p_{SW}\|} J^W \dot{q} \right) \\ &= \frac{e_{SW}^T e_r}{\|k_x\|} e_y^T J^W \dot{q}. \end{aligned} \quad (38)$$

This means the Jacobian with respect to the wrist is

$$\begin{aligned} J_{\psi, W} &= \frac{e_{SW}^T e_r}{\|k_x\|} e_y^T + \frac{e_{SW}^T e_t^\times e_r}{\|k_x\|} e_x^T \\ &\quad - \frac{e_{SW}^T p_{SE}}{\|p_{SW}\| \|p_{CE}\|} (e_{SW}^\times e_{CE})^T \end{aligned} \quad (39)$$

As expected based on the previous singularity analysis, other than the $p_{SW} = 0$ and $p_{CE} = 0$ conditions from the general SEW angle, J_ψ is only undefined when $k_x = 0$.

In deriving the Jacobian, we made no assumptions on the norms or orthogonality of e_r or e_t . Setting $e_t = 0$ lets us recover the Jacobian for the conventional SEW angle.

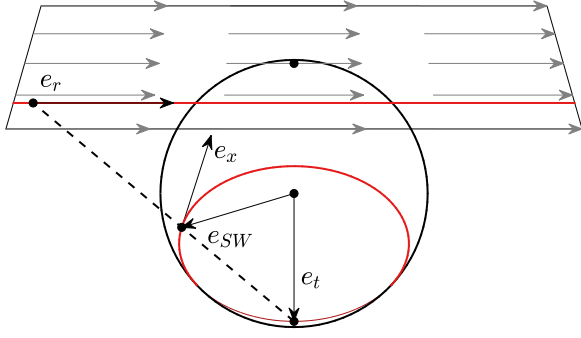


Figure 8. The stereographic projection of e_r onto e_{SW} is e_x , where the pole of the projection is at e_t .

5.2 Relationship to Stereographic Projection

The stereographic SEW angle gets its name from stereographic projection, which is a type of one-to-one mapping between points on a sphere and a plane (Needham 1997). Stereographic projection has the following geometric definition: Pick a point on the sphere as the pole of the projection and place the plane tangent to the sphere at the antipodal point. Corresponding points on the sphere and plane are collinear with the pole.

We can show the reference direction e_x for the stereographic SEW angle is generated by performing a stereographic projection of a constant vector field onto a unit sphere (Figure 8). For any choice of e_t and e_r , we can generate a constant vector field in the e_r direction on the projection plane and place the projection pole at e_t . Then, for any choice of e_{SW} , we can form a projection line passing through e_t and e_{SW} and intersecting with the projection plane. The projection of e_r onto the sphere is then the vector which is tangent to the circle formed by the intersection of the unit sphere and the plane which contains the tips of e_t and e_{SW} and is parallel to e_r . This plane is normal to k_{rt} , and so the projection of e_r from the plane to the sphere is e_x .

5.3 Preservation of Angles

Although it appears that we have three DOF in picking the parameters for the stereographic SEW angle (two DOF for e_t and one remaining DOF for e_r), we can show that the one DOF for e_r does not change the behavior of the SEW angle; it only changes the angle by a constant. Changing the angle of e_r around e_t is equivalent to changing the SEW angle ψ by the same angle.

Since stereographic projection is a conformal mapping, changes of angles in the projection plane get preserved after projecting onto the unit sphere. This means changing the angle of e_r on the projection plane corresponds to an equal change of angle to e_x and e_y .

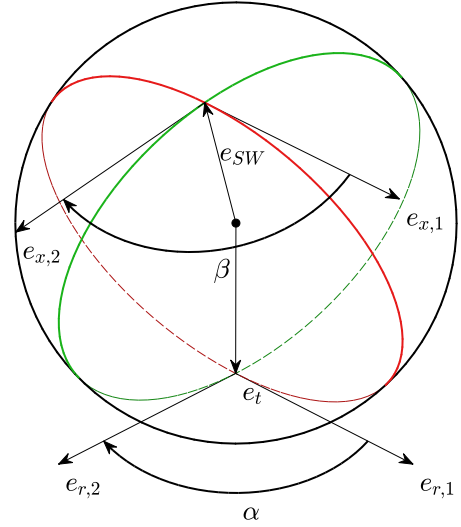


Figure 9. $e_{x,i}$ is tangent to the circle generated from the plane through e_t , $e_t + e_{r,i}$ and e_{SW} . The angles of intersections of any two circles on a sphere are equal. Therefore, $\alpha = \beta$.

We can also prove this preservation of angles property directly (Figure 9). First, set $e_r = e_{r,1}$, which results in $e_{x,1}$. This vector is tangent to the circle which is tangent to $e_{r,1}$ and is passing through e_{SW} and e_t . Now, pick a new $e_r = e_{r,2}$ which is $e_{r,1}$ rotated by an angle α about $-e_t$. This generates $e_{x,2}$ which is tangent to the circle passing through e_{SW} and e_t but tangent to $e_{r,2}$. The angle from $e_{x,1}$ to $e_{x,2}$ about e_{SW} is an angle β . The angles of intersection of any two circles on a sphere are equal, so $\alpha = \beta$.

The preservation of angles property can aid in analyzing the behavior of SEW angle when only q_1 changes in the typical case of $e_t = -h_1$, which occurs when the first joint of the robot is pointing up and the singularity direction is chosen to point down. In this case, when q_1 changes but all other joint angles are held constant, ψ changes at the same rate. This means the first element of J_ψ is always 1.

We can compare this to the conventional SEW angle where $e_r = h_1$. In this case, the SEW angle does not change when only q_1 changes. (The conventional SEW angle has rotational invariance about e_r .) This means the first element of J_ψ is always 0.

5.4 Singularity Behavior

The singularity for the stereographic SEW angle is of order two. This means that if e_{SW} travels in a small circle around e_t , e_x rotates twice for each rotation of e_{SW} . This is unlike the conventional SEW angle, where each singularity is of order one.

Although a singularity of order two would result in larger elbow motion than a singularity of order one for a fixed SEW angle as e_{SW} passes close to e_t , large motion disappears if e_{SW} passes directly through e_t in a smooth

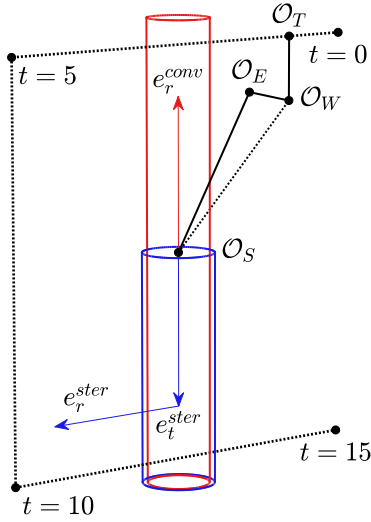


Figure 10. Task-space trajectory for the comparison demonstration. The end effector position follows three line segments while the end effector rotation and SEW angle are constant. The red and blue cylinders indicate the conventional and stereographic SEW angle singularity directions, respectively.

path. As a path gets closer to the singularity, e_x gets closer to making a full revolution of 2π radians. At the limit, the elbow rotates by exactly 2π , which is equivalent to not rotating at all. We can compare this to the conventional SEW angle, where passing through the singularity in a smooth path causes e_x to rotate by π radians.

5.5 Comparison Demonstration

Two joint trajectories were generated for a KUKA LBR iiwa 14 R820 robot (KUKA 2022) with constants $R_{07} = I$ and $\psi = \pi/4$: One using the conventional SEW angle with $e_r = [0 \ 0 \ 1]^T$, and the other using the stereographic SEW angle with $e_t = [0 \ 0 \ -1]^T$ and $e_r = [0 \ 1 \ 0]^T$. The task-space trajectory for p_{0T} took a straight-line path through 4 points, with $x = \pm 0.40$ m, $y = 0.01$ m, and $z = 0.36 \pm 0.40$ m. There was a small offset in the y direction as otherwise there would not be any large joint motion for the stereographic SEW angle. For each trajectory, the initial pose was picked such that $q_2 > 0$, $q_4 > 0$, and $q_6 > 0$. The task-space trajectory is shown in Figure 10, and the results are shown in Figure 11 (Extension 1).

For the conventional SEW angle, the singularities occur near $e_{SW} = \pm[0 \ 0 \ 1]^T$. In following the trajectory with the conventional SEW angle, there were large joint motions in two places, each corresponding to the positive and negative direction.

For the stereographic SEW angle, the singularity only occurs near $e_{SW} = [0 \ 0 \ -1]^T$. We see that the large joint motion only occurred at one time in the trajectory. The

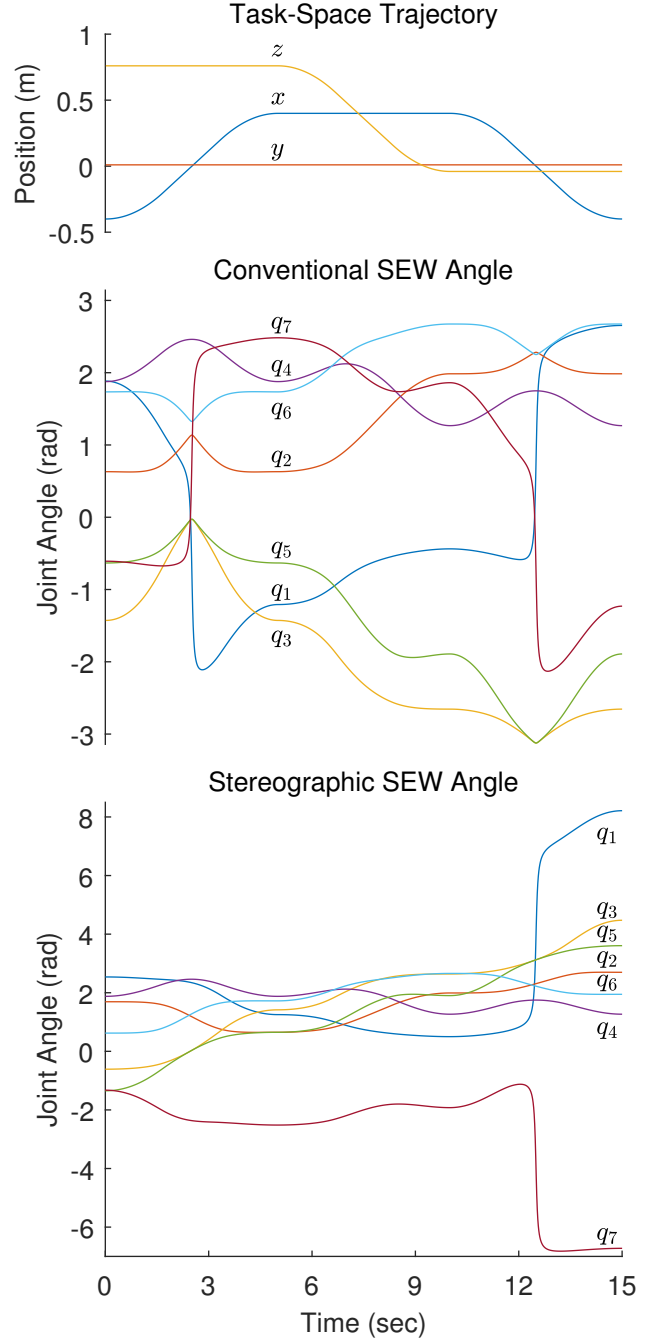


Figure 11. Joint-space trajectories using constant conventional or stereographic SEW angles. Whereas the conventional SEW angle results in large joint motion when the wrist passes near a line, the stereographic SEW angle results in large joint motion when passing near a half-line. This unidirectional singularity region occurs below the robot ($z < 0$) and cannot typically be reached. (See also Extension 1.)

joint motion was also larger than in the conventional SEW case, as the singularity is of order two instead of one. The singularity occurs when the wrist is below the base, which in many cases would be out of the feasible workspace.

6 Inverse Kinematics

6.1 Problem Formulation

The inverse kinematics problem for a 7R robot arm is to find all possible joint angles q corresponding to an end effector pose and SEW angle (R_{0T}, p_{0T}, ψ) given the robot kinematic parameters $(\{p_{i-1,i}\}_{i=1}^7, p_{7T}, \{h_i\}_{i=0}^7, R_{7T})$ and stereographic SEW parameters $(e_r, e_t, p_{iS}, p_{jE}, p_{kW})$. These inverse kinematics solutions are agnostic to the SEW formulation, and so the conventional SEW angle definition may be used instead.

The inverse kinematics procedures can apply not just to 7-DOF manipulators, but also to 6-DOF manipulators which have been provided an extra degree of freedom, say, by being placed on an omnidirectional mobile base with the location of the origin of the base specified. For example, if we use a UR5 robot (Universal Robots 2022), tilt the robot so the first joint is not vertical, and pick the origin of the mobile base to be directly under the intersection of joints 1 and 2, then the system becomes a 3R-R-2R-R or 3R-2R||-2R robot.

To find the inverse kinematics of a 7-DOF robot where the redundant degree of freedom is parameterized by some joint angle q_i , find the 6-DOF robot generated by fixing q_i and refer to the inverse kinematics procedures provided in Elias and Wen (2024).

Without loss of generality, assume $p_{01} = 0$. (Otherwise, subtract p_{01} from p_{0T} and p_{0S} .) Rewrite the kinematics equations in terms of R_{07} and p_{07} , which can be immediately calculated:

$$R_{07} = R_{0T}R_{7T}^T = R_{01}R_{12}R_{23}R_{34}R_{45}R_{56}R_{67}, \quad (40a)$$

$$\begin{aligned} p_{07} &= p_{0T} - R_{07}p_{7T} \\ &= R_{01}p_{12} + R_{02}p_{23} + R_{03}p_{34} \\ &\quad + R_{04}p_{45} + R_{05}p_{56} + R_{06}p_{67}. \end{aligned} \quad (40b)$$

The inverse kinematics procedures can now be written in terms of (R_{07}, p_{07}, ψ) . If the shoulder is constant in the 0 frame and the wrist is constant in the 7 frame, then we can use (9) to find n_{SEW} since ψ is given p_{SW} is known:

$$p_{SW} = p_{07} + R_{07}p_{7W} - p_{0S}. \quad (41)$$

A key step in the inverse kinematics procedure is to find the elbow location, i.e., p_{SE} . This sometimes involves finding the shoulder angle θ_S or the wrist angle θ_W , defined as

$$p_{SE} = R(n_{SEW}, \theta_S)e_{SW} \|p_{SE}\|, \quad (42)$$

$$p_{EW} = R(n_{SEW}, \theta_W)e_{SW} \|p_{EW}\|. \quad (43)$$

Note that for a given shoulder position, wrist position, and SEW angle, the elbow must be somewhere in a half plane: Given n_{SEW} and e_{CE} , we require $n_{SEW}^T p_{SE} = 0$ and $e_{CE}^T p_{SE} > 0$. To place the elbow in the correct half plane,

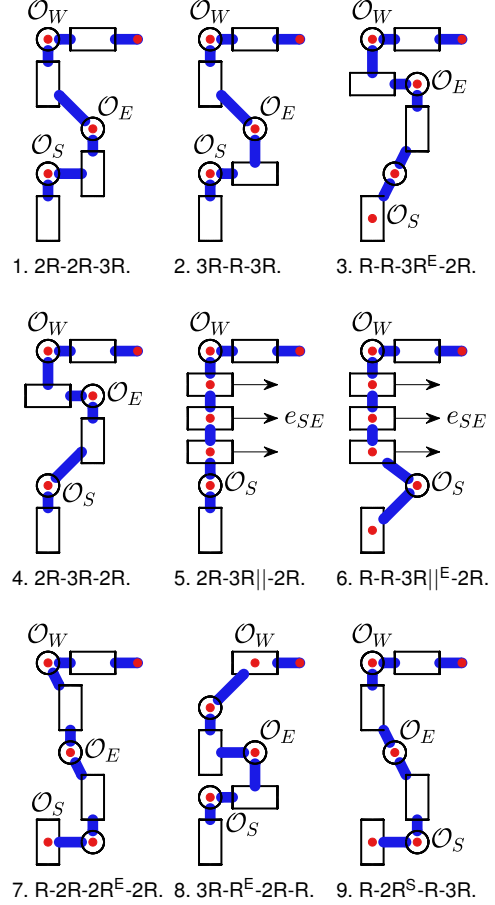


Figure 12. Examples of robots in kinematic families with closed-form and 1D search solutions.

$\theta_S \in [0, \pi]$ and $\theta_W \in [-\pi, 0]$. A singularity occurs when $\theta_S = 0$ or $\theta_W = 0$, as this corresponds to the shoulder, elbow, and wrist being collinear.

A number of inverse kinematics solutions are provided below, and the different kinematic families, along with examples of specific robots for some types, are shown in Table 3 and Figure 12. There exist many other kinematic families, but we include enough examples to demonstrate the technique of applying the subproblem decomposition method to solve the inverse kinematics problem. The reader is referred to the discussions in Elias and Wen (2024) for information regarding handling multiple branches, extraneous solutions, least-squares solutions, 1D and 2D searches, and internal and boundary singularities.

Closed-form solutions may exist when a robot has 3R or 3R|| joints, as a 3R joint may result in decoupling between position and orientation, and a 3R|| joint is the limit of a 3R joint as the point of intersection moves infinitely far away. (It only makes sense to place O_E infinitely far away, as placing O_S or O_W infinitely far away results in e_{SW}

Table 3. Kinematic families of robots with IK solutions demonstrated in this paper. The Motoman SIA50D appears as two examples since one robot may be part of multiple kinematic families.

IK Type	Kinematic Family	Robot Example
Closed-Form	1. 2R-2R-3R	FREND (Debus and Dougherty 2009) KUKA LBR iiwa 14 R820 (KUKA 2022)
	2. 3R-R-3R	Motoman SIA5D (Yaskawa 2022b)
	3. R-R-3R ^E -2R	Motoman SIA50D (Yaskawa 2022a)
	4. 2R-3R-2R	
	5. 2R-3R -2R	SSRMS (Crane III, Duffy and Carnahan 1991) SPDM (Mukherji, Ray, Stieber and Lymer 2001) ERA (Boumans and Heemskerk 1998)
	6. R-R-3R ^E -2R	
1D Search	7. R-2R-2R ^E -2R	Sawyer (Rethink Robotics 2022) Baxter (Rethink Robotics 2015) OSAM-2 (Motiv Space Systems 2022) OB7 (Productive Robots 2023)
	8. 3R-R ^E -2R-R	Franka Production 3 (Franka Emika 2022) xArm7 (Ufactory 2022)
	9. R-2R ^S -R-3R	Motoman SIA50D (Yaskawa 2022a)
2D Search	10. General 7-DOF	ABB Yumi (ABB 2022) RRC (Robotics Research Corporation 2005)

being a constant vector in the base or end effector frame.) In other cases, the solution requires a 1D or 2D search over q_i , θ_S , or θ_W . We also demonstrate converting a search-based solution into a polynomial root finding problem using the tangent half-angle substitution in Section 6.4.

A common step in the IK solutions below is to solve the orientation of a 3R joint. To solve such a spherical joint (shown here at the robot wrist)

$$R_{45}R_{56}R_{67} = R_{47}, \quad (44)$$

first solve for (q_5, q_6) using Subproblem 2

$$R_{56}h_7 = R_{54}R_{47}h_7. \quad (45)$$

Then, solve for q_7 using Subproblem 1:

$$R_{67}p = R_{65}R_{54}R_{47}p, \quad (46)$$

where p is any vector not collinear with h_7 .

In the following IK solutions, always pick the origins of intersecting axes for that kinematic family to be coincident. For example, in a 3R-R-3R robot, pick $\mathcal{O}_1 = \mathcal{O}_2 = \mathcal{O}_3 = \mathcal{O}_S$, which means $p_{12} = p_{23} = p_{0S} = 0$. When an elbow is made of parallel joints (say, that include joint 3), pick $p_{SE} = e_{SE} = R_{02}h_3$.

6.2 IK Solutions

6.2.1 2R-2R-3R Arm

The position equation becomes

$$p_{07} = p_{SW} = R_{02}(p_{23} + R_{24}p_{45}), \quad (47)$$

and given θ_S we have

$$R_{02}p_{23} = \mathbf{R}(n_{SEW}, \theta_S)e_{SW} \|p_{23}\|. \quad (48)$$

Use Subproblem 3 to find $\theta_S \in [0, \pi]$:

$$\|\mathbf{R}(n_{SEW}, \theta_S)e_{SW} \|p_{23}\| - p_{07}\| = \|p_{45}\|. \quad (49)$$

Find (q_1, q_2) using Subproblem 2:

$$R_{12}p_{23} = R_{10}\mathbf{R}(n_{SEW}, \theta_S)e_{SW} \|p_{23}\|. \quad (50)$$

Similarly, find (q_3, q_4) using Subproblem 2:

$$R_{32}(R_{21}R_{10}p_{07} - p_{24}) = R_{34}p_{45}. \quad (51)$$

Finally, find (q_5, q_6, q_7) by solving the spherical wrist:

$$R_{45}R_{56}R_{67} = (R_{01}R_{12}R_{23}R_{34})^T R_{07}. \quad (52)$$

6.2.2 3R-R-3R Arm

The position equation becomes

$$p_{07} = p_{SW} = R_{03}(p_{34} + R_{34}p_{45}). \quad (53)$$

Solve for up to two solutions of q_4 using Subproblem 3:

$$\|R_{34}p_{45} + p_{34}\| = \|p_{07}\|. \quad (54)$$

Represent R_{03} as three consecutive orthogonal rotations:

$$R_{03} = \mathbf{R}(e_{SW}, \theta_a)\mathbf{R}(n_{SEW}, \theta_b)\mathbf{R}(e_{SW}, \theta_c). \quad (55)$$

There are up to two solutions for $(\theta_a, \theta_b, \theta_c)$, but they represent the same R_{03} , so only keep one solution. Solve

for (θ_b, θ_c) using Subproblem 2:

$$\mathbf{R}(n_{SEW}, \theta_b)^T p_{07} = \mathbf{R}(e_{SW}, \theta_c)(p_{34} + R_{34}p_{45}). \quad (56)$$

Then, use Subproblem 4 to find θ_a , keeping only the solutions that place the elbow in the correct half plane:

$$n_{SEW}^T \mathbf{R}(e_{SW}, \theta_a) \mathbf{R}(n_{SEW}, \theta_b) \mathbf{R}(e_{SW}, \theta_c) p_{3E} = 0. \quad (57)$$

Find (q_1, q_2, q_3) by solving the spherical shoulder:

$$R_{01}R_{12}R_{23} = \mathbf{R}(e_{SW}, \theta_a) \mathbf{R}(n_{SEW}, \theta_b) \mathbf{R}(e_{SW}, \theta_c). \quad (58)$$

Similarly, find (q_5, q_6, q_7) by solving (52).

6.2.3 R-R-3R^E-2R Arm

Write θ_W as

$$R_{05}p_{56} = \mathbf{R}(n_{SEW}, \theta_W) e_{SW} \|p_{56}\|. \quad (59)$$

Using Subproblem 5, we can find up to four solutions of (q_1, q_2, θ_W) , where $\theta_W \in [-\pi, 0]$:

$$p_{07} - \mathbf{R}(n_{SEW}, \theta_W) e_{SW} \|p_{56}\| = R_{01}(p_{12} + R_{12}p_{23}). \quad (60)$$

Next, find up to two solutions of (q_6, q_7) using Subproblem 2:

$$R_{67}R_{07}^T \mathbf{R}(n_{SEW}, \theta_W) e_{SW} \|p_{56}\| = R_{65}p_{56}. \quad (61)$$

To solve for (q_3, q_4, q_5) , solve the spherical elbow:

$$R_{23}R_{34}R_{45} = (R_{01}R_{12})^T R_{07}(R_{56}R_{67})^T. \quad (62)$$

6.2.4 2R-3R-2R Arm

Find $\theta_S \in [0, \pi]$ using Subproblem 3:

$$\|\mathbf{R}(n_{SEW}, \theta_S) e_{SW} \|p_{23}\| - p_{07}\| = \|p_{56}\|. \quad (63)$$

Find (q_1, q_2) with Subproblem 2 to solve (50). Similarly, find (q_6, q_7) :

$$R_{67}R_{07}^T(p_{07} - R_{02}p_{23}) = R_{65}p_{56}. \quad (64)$$

Find (q_3, q_4, q_5) by solving (62).

6.2.5 2R-3R||-2R Arm

This robot is the limit of a 2R-3R-2R arm where the intersection point of the elbow joint moves to infinity. We can write

$$R_{01}R_{12}h_3 = \mathbf{R}(n_{SEW}, \theta_S) e_{SW}. \quad (65)$$

Combining with the position equation gives

$$h_3^T(p_{23} + p_{34} + p_{45} + p_{56}) = h_3^T R_{02}^T p_{07}. \quad (66)$$

Solve for $\theta_S \in [0, \pi]$ using Subproblem 4:

$$e_{SW}^T \mathbf{R}(n_{SEW}, \theta_S)^T p_{07} = h_3^T(p_{23} + p_{34} + p_{45} + p_{56}). \quad (67)$$

Find (q_1, q_2) using Subproblem 2:

$$R_{12}h_3 = R_{10} \mathbf{R}(n_{SEW}, \theta_S) e_{SW}. \quad (68)$$

Find $(q_3 + q_4 + q_5, q_6, q_7)$ by solving a spherical joint:

$$R_{25}R_{56}R_{67} = R_{02}^T R_{07}. \quad (69)$$

Use Subproblem 3 to find q_4 :

$$\|p_{34} + R_{34}p_{45}\| = \|R_{02}^T p_{07} - p_{23} - R_{25}p_{56}\|. \quad (70)$$

Use Subproblem 1 to find q_3 :

$$R_{23}(p_{34} + R_{34}p_{45}) = R_{02}^T p_{07} - p_{23} - R_{25}p_{56}. \quad (71)$$

Find q_5 with subtraction, wrapping to $[-\pi, \pi]$ if desired.

6.2.6 R-R-3R||^E-2R Arm

This is a more general version of a 2R-3R||-2R robot. Use Subproblem 6 to find (θ_S, q_2) , where $\theta_S \in [0, \pi]$:

$$e_{SW}^T \mathbf{R}(n_{SEW}, \theta_S)^T p_{07} - h_3^T R_{21}p_{12} = h_3^T(p_{23} + p_{34} + p_{45} + p_{56}), \quad (72a)$$

$$h_1^T \mathbf{R}(n_{SEW}, \theta_S) e_{SW} - h_1^T R_{12}h_3 = 0. \quad (72b)$$

Use Subproblem 1 to find q_1 solving (65). Find $(q_3 + q_4 + q_5, q_6, q_7)$ by solving a spherical joint (69). Use Subproblem 3 to find q_4 :

$$\|p_{34} + R_{34}p_{45}\| = \|R_{02}^T p_{07} - R_{21}p_{12} - p_{23} - R_{25}p_{56}\|. \quad (73)$$

Use Subproblem 1 to find q_3 :

$$R_{23}(p_{34} + R_{34}p_{45}) = R_{02}^T p_{07} - R_{21}p_{12} - p_{23} - R_{25}p_{56}. \quad (74)$$

Find q_5 with subtraction, wrapping to $[-\pi, \pi]$ if desired.

6.2.7 R-2R-2R^E-2R Arm (1D Search)

Given θ_W , we can write

$$R_{05}p_{56} = \mathbf{R}(n_{SEW}, \theta_W) e_{SW} \|p_{56}\|. \quad (75)$$

Then, find q_1 using Subproblem 3:

$$\|R_{01}p_{12} - p_{07} + R_{05}p_{56}\| = \|p_{34}\|. \quad (76)$$

Find (q_2, q_3) using Subproblem 2:

$$R_{23}p_{34} = R_{21}(R_{10}p_{07} - R_{10}R_{05}p_{56} - p_{12}). \quad (77)$$

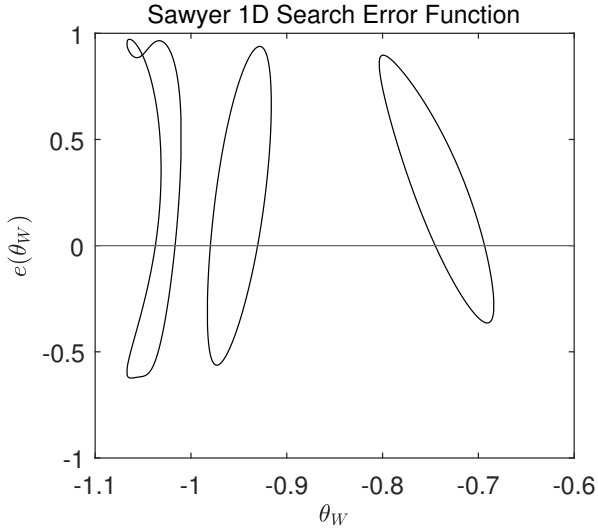


Figure 13. Error function for a Sawyer (R-2R-2R^E-2R) arm. This function has eight branches, although only four are seen for this pose. A 1D search may be used to find the zeros, which correspond to IK solutions.

Find (q_4, q_5) using Subproblem 2:

$$R_{45}p_{56} = R_{43}(R_{32}R_{21}(R_{10}p_{07} - p_{12}) - p_{34}). \quad (78)$$

The error is a metric of solvability of

$$R_{56}R_{67} = R_{05}^T R_{07}. \quad (79)$$

By projecting onto h_6 and h_7 , we get the error

$$e(\theta_W) = h_6^T R_{05}^T R_{07} h_7 - h_6^T h_7. \quad (80)$$

Search over $\theta_W \in [-\pi, 0]$ to find all solutions of $e(\theta_W) = 0$. For each solution θ_W , calculate q_6 and q_7 using Subproblem 1:

$$R_{56}h_7 = R_{05}^T R_{07} h_7, \quad (81)$$

$$R_{76}h_6 = R_{07}^T R_{05} h_6. \quad (82)$$

A Sawyer arm example is shown in Figures 13 and 14 (Extension 2).

6.2.8 3R-R^E-2R-R Arm (1D Search)

Given $\theta_S \in [0, \pi]$, we have

$$R_{03}p_{34} = \mathbf{R}(n_{SEW}, \theta_S) e_{SW} \|p_{34}\|. \quad (83)$$

Use Subproblem 3 to find q_7 from

$$\|R_{07}^T(p_{07} - R_{03}p_{34}) - R_{76}p_{67}\| = \|p_{45}\|. \quad (84)$$

Then, solve (q_5, q_6) using Subproblem 2:

$$R_{54}p_{45} = R_{56}(R_{67}R_{07}^T(p_{07} - R_{03}p_{34}) - p_{67}). \quad (85)$$

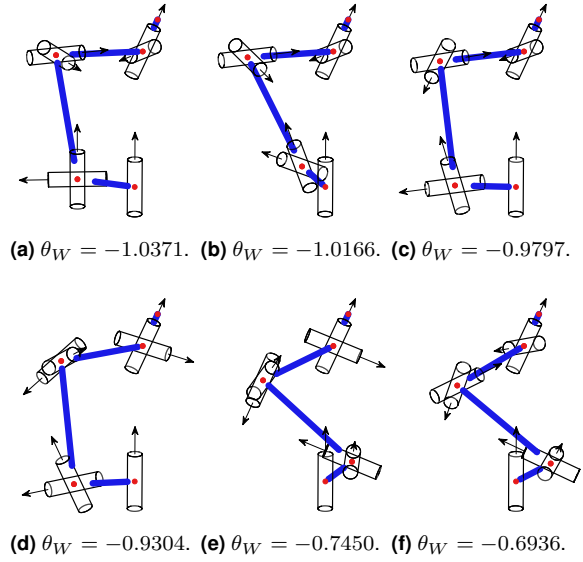


Figure 14. Six IK solutions for a Sawyer (R-2R-2R^E-2R) arm corresponding to the zeros of the error shown in Figure 13.

We have the identity

$$R_{43}p_{34} = R_{47}R_{07}^T R_{03}p_{34}, \quad (86)$$

which may be expressed as an error function in terms of θ_S :

$$e(\theta_S) = h_4^T (p_{34} - R_{47}R_{07}^T R_{03}p_{34}). \quad (87)$$

Search over $\theta_S \in [0, \pi]$ to find the zeros of this error. For each solution θ_S , find q_4 with Subproblem 1, then find (q_1, q_2, q_3) by solving the spherical shoulder:

$$R_{01}R_{12}R_{23} = R_{07}(R_{34}R_{45}R_{56}R_{67})^T. \quad (88)$$

6.2.9 R-2R^S-R-3R Arm (1D Search)

Given $q_1 \in [-\pi, \pi]$, solve for q_4 using Subproblem 3:

$$\|p_{34} + R_{34}p_{45}\| = \|R_{10}p_{07} - p_{12}\|. \quad (89)$$

Solve for (q_2, q_3) using Subproblem 2:

$$R_{21}(R_{10}p_{07} - p_{12}) = R_{23}(p_{34} + R_{34}p_{45}). \quad (90)$$

Find the shoulder-elbow vector $p_{SE} = R_{03}p_{34}$, from which we can calculate the error for ψ in terms of q_1 . A plot of this error is a good graphical tool to determine what range of SEW angle is feasible for a given end effector pose. For each solution q_1 , find (q_5, q_6, q_7) by solving (52).

6.2.10 General 7-DOF Arm (2D Search)

Pick $\mathcal{O}_1 = \mathcal{O}_S$, $\mathcal{O}_4 = \mathcal{O}_E$, and $\mathcal{O}_7 = \mathcal{O}_W$. The shoulder, elbow, and wrist may be placed arbitrarily as in Figure 2

and the solution will remain similar. Given (q_1, q_2) , find q_3 using Subproblem 4, keeping only solutions which place the elbow in the correct half plane:

$$n_{SEW}^T R_{02} R_{23} p_{34} = -n_{SEW}^T (R_{01} p_{12} + R_{02} p_{23}). \quad (91)$$

Then, find (q_5, q_6, q_7) with Subproblem 5 to solve

$$-p_{67} + R_{67} R_{07}^T (p_{07} - p_{14}) = R_{65} (p_{56} + R_{54} p_{45}), \quad (92)$$

and find the error

$$e(q_1, q_2) = \|R_{03}^T R_{07} R_{47}^T h_4 - h_4\|. \quad (93)$$

Search over (q_1, q_2) to find zeros of this error. Then, find q_4 using Subproblem 1:

$$R_{34} p = R_{03}^T R_{07} R_{47}^T p, \quad (94)$$

where p is any vector not collinear with h_4 .

6.3 Continuous and Least-Squares IK

Using the subproblem decomposition approach means that continuous non-exact solutions for q are returned even for branches where the solution does not exist, as discussed in Elias and Wen (2024). Therefore, IK is numerically stable for paths where the robot switches branches by passing through a boundary singularity.

For some special cases, the IK solution is also the solution to the global least-squares IK problem, which is posed as

$$\begin{aligned} \min_q & \|p_{0T}(q) - p_{0T}^{des}\| \\ \text{s.t. } & R_{0T}(q) = R_{0T}^{des}, \quad \psi(q) = \psi^{des} \end{aligned} \quad (95)$$

where $(R_{0T}^{des}, p_{0T}^{des}, \psi^{des})$ is the desired end effector pose and SEW angle. For some robots, the $\psi(q) = \psi^{des}$ constraint cannot be achieved when at a boundary singularity because the self-motion manifold degenerates to a point, and so this constraint must be dropped when $p_{0T}(q) \neq p_{0T}^{des}$.

3R-R-3R, 2R-3R-2R, and 2R-2R-3R arms can all achieve least-squares inverse kinematics if the task frame is at the wrist center ($p_{7T} = 0$), all 2R joints have a spherical workspace ($h_i^T h_{i+1} = h_{i+1}^T p_{i+1, i+2} = 0$) and all 3R joints can achieve any orientation ($h_i^T h_{i+1} = h_{i+1}^T h_{i+2} = 0$).

For a 3R-R-3R arm, since rotation of the whole arm is always possible between the spherical shoulder and wrist, the self-motion manifold does not degenerate to a point at boundary singularities. Therefore, \mathcal{O}_E should be placed such that it is not collinear with \mathcal{O}_S and \mathcal{O}_W at the workspace boundary. (Using $p_{SE} = e_{SE} = R_{03} h_4$ may also be a good option.)

For 2R-3R-2R and 2R-2R-3R arms, the robot's self-motion manifold degenerates into a point at boundary

singularities, so although the SEW angle will be undefined at the boundary singularity, the SEW angle is not needed. This also means the SEW angle constraint in (95) must be dropped.

6.4 Polynomial Method

The tangent half-angle substitution $x_i = \tan(q_i/2)$ can be used to convert a search-based solutions into a system of multivariate polynomials. By eliminating all but one variable, we obtain a high-order polynomial in the tangent half-angle of one joint. After finding roots of this polynomial, the remaining joint angles are found in closed-form. Although this procedure is not as computationally efficient as 1D or 2D search, it does give a stronger guarantee of finding all solutions. We demonstrate solving IK using the polynomial method for the Sawyer (R-2R-2R^E-2R) arm according to the procedure described in Elias and Wen (2024).

To improve computational performance, we reduce the number of variables and search over a joint angle rather than θ_W . The downside is that we must check for extraneous solutions where the elbow is in the wrong half-plane.

Given q_7 , find q_6 using Subproblem 4:

$$(R_{67} R_{07}^T n_{SEW})^T R_{65} p_{56} = n_{SEW}^T p_{07}. \quad (96)$$

Then, find q_1 with Subproblem 3 according to (76), where $R_{05} = R_{07} R_{76} R_{65}$. Although Subproblem 2 could be used to find q_2 and q_3 using (77), we instead first solve for q_2 with Subproblem 4 to solve

$$h_3^T R_{21} (R_{10} p_{07} - R_{10} R_{05} p_{56} - p_{12}) = h_3^T p_{34}, \quad (97)$$

and then find q_3 with Subproblem 1. This allows us to eliminate x_3 from the system of polynomials. The error is

$$e(q_7) = h_4^T R_{03}^T R_{07} R_{57}^T h_5 - h_4^T h_5. \quad (98)$$

For all solutions of $e(q_7) = 0$, we can find q_4 and q_5 with Subproblem 1:

$$R_{34} h_5 = R_{03}^T R_{07} R_{57}^T h_5, \quad (99)$$

$$R_{54} h_4 = R_{57} R_{07}^T R_{03} h_4. \quad (100)$$

The Sawyer kinematics parameters (in mm) are:

$$\begin{aligned} h_1 &= [0 \ 0 \ 1]^T, & h_2 &= h_4 = h_6 = [0 \ 1 \ 0]^T, \\ h_3 &= h_5 = h_7 = [1 \ 0 \ 0]^T, \\ p_{12} &= [81 \ 192.5 \ 0]^T, & p_{23} &= p_{45} = p_{67} = 0, \\ p_{34} &= [400 \ -168.5 \ 0]^T, & p_{56} &= [400 \ 136.3 \ 0]^T. \end{aligned} \quad (101)$$

Using the conventional SEW angle, we pick the following example pose (in mm):

$$\begin{aligned} R_{06} &= I_3, & p_{06} &= [500 \ 500 \ 250]^T, \\ \psi &= 0, & e_r &= [0 \ 0 \ 1]^T. \end{aligned} \quad (102)$$

Table 4. Sawyer IK solutions using the polynomial method.

#	q_1	q_2	q_3	q_4	q_5	q_6	q_7
1	0.7012115792	-0.9732888736	-0.09318675442	1.466219046	1.023549438	-0.7523604269	-0.8108011807
2	-1.187806104	-2.406581118	2.111970078	1.816987670	1.723460652	-0.7764631130	-0.7042361521
3	-0.4801904691	-1.230875621	-2.301720627	-2.019222054	-2.695866355	-0.8165545740	-0.5807494539
4	-2.104051752	-2.319400366	-0.7687046831	-0.5435788511	2.572212359	0.7314410389	0.9764868428
5	0.7028860908	-1.034458755	0.05293672172	0.9219195962	-1.476315039	0.7522268563	1.404840771
6	-1.439122724	-2.605604387	1.821941574	0.9918815495	-0.4713994287	0.7552919261	1.423570856
7	-0.2361394798	-1.013327345	-2.064532180	-1.375427168	1.007651470	0.8154933152	1.682578759

The stereographic SEW angle can be used just as easily since the solution only depends on n_{SEW} .

After converting all subproblems and the error equation using the tangent half-angle identity, we find four equations in four unknowns with (23, 42, 5, 291) terms, respectively:

$$\begin{aligned} P_1(x_1, x_6, x_7) &= 0, & P_2(x_1, x_2, x_6, x_7) &= 0, \\ P_3(x_6, x_7) &= 0, & P_4(x_1, x_2, x_6, x_7) &= 0. \end{aligned} \quad (103)$$

Eliminating all variables but x_7 , we find a resultant univariate polynomial of degree 48. Of the 16 real solutions, 7 correspond to solutions to the IK problem, and the other 9 solutions correspond to poses with $\psi = \pi$. All 7 IK solutions for this pose are shown in Table 4 to 10 significant figures.

7 Conclusion

We have introduced the general SEW angle which allows us to analyze the behavior of the conventional SEW angle but with an arbitrary reference direction function. A special choice of the reference direction function, the stereographic SEW angle, reduces the effect of the coordinate singularity as compared to the conventional SEW angle. The stereographic SEW angle allows the use of more of the workspace without encountering singularities. Even at a singularity, the arm can have continuous joint movement as long as a smooth path is taken directly through the singularity. We have shown that since an algorithmic singularity is unavoidable for any choice of parameterization of the redundant degree of freedom, the stereographic SEW angle is ideal in that it only encounters a singularity when the wrist is at a half-line from the shoulder.

We have also used the subproblem decomposition method to provide IK solutions for most known 7R robots. These solutions are often closed-form and may sometimes require a 1D or 2D search. This method finds all IK solutions and finds least-squares solutions for some robots as well. We provide IK solutions for both common robots as well as robots which do not seem to be manufactured yet, such as an R-R-3R||-2R arm. Furthermore, we are the first to demonstrate solving IK by finding a high-order polynomial in the tangent half-angle for 7R arms parameterized by the general SEW angle.

In the future, it would be interesting to further investigate resolving redundancy given this new parameterization, that is, picking the ideal trajectory for the stereographic SEW angle. It may also be worthwhile to further investigate IK for more types of 7R robots using the subproblem decomposition approach.

Declaration of conflicting interests

The authors declare that there is no conflict of interest.

Funding

The author(s) received no financial support for the research, authorship, and/or publication of this article.

References

- ABB (2022) IRB 14000 YuMi - collaborative robot. <https://new.abb.com/products/robotics/collaborative-robots/yumi/irb-14000-yumi>. (accessed Oct. 31, 2022).
- An HH, Clement WI and Reed B (2014) Analytical inverse kinematic solution with self-motion constraint for the 7-DOF restore robot arm. In: *2014 IEEE/ASME International Conference on Advanced Intelligent Mechatronics*. IEEE, pp. 1325–1330.
- Baillieul J (1985) Kinematic programming alternatives for redundant manipulators. In: *Proceedings. 1985 IEEE International Conference on Robotics and Automation*, volume 2. IEEE, pp. 722–728.
- Baillieul J, Hollerbach J, Brockett R, Martin D, Percy R and Thomas R (1987) Kinematically redundant robot manipulators. In: *Proceedings of the Workshop on Space Telerobotics*, volume 2. Jet Propulsion Lab., California Inst. of Tech., pp. 245–255.
- Boumans R and Heemskerk C (1998) The European robotic arm for the international space station. *Robotics and Autonomous systems* 23(1-2): 17–27.
- Burdick J and Seraji H (1989) Characterization and control of self-motions in redundant manipulators. In: *Proceedings of the NASA Conference on Space Telerobotics, Volume 2*. pp. 3–14.

- Carignan CR and Howard RD (2000) A partitioned redundancy management scheme for an eight-joint revolute manipulator. *Journal of Robotic Systems* 17(9): 453–468.
- Carignan CR, Lane JC and Churchill PJ (2001) Controlling robots on-orbit. In: *Proceedings 2001 IEEE International Symposium on Computational Intelligence in Robotics and Automation (Cat. No. 01EX515)*. IEEE, pp. 314–319.
- Chen Y, Zhang X, Huang Y, Wu Y and Ota J (2023) Kinematics optimization of a novel 7-DOF redundant manipulator. *Robotics and Autonomous Systems* 163: 104377.
- Chiaverini S (1997) Singularity-robust task-priority redundancy resolution for real-time kinematic control of robot manipulators. *IEEE Transactions on Robotics and Automation* 13(3): 398–410.
- Choi Y, Oh Y, Oh SR, Park J and Chung WK (2004) Multiple tasks manipulation for a robotic manipulator. *Advanced Robotics* 18(6): 637–653.
- Crane III CD, Duffy J and Carnahan T (1991) A kinematic analysis of the space station remote manipulator system (SSRMS). *Journal of Robotic Systems* 8(5): 637–658.
- Debus T and Dougherty S (2009) Overview and performance of the front-end robotics enabling near-term demonstration (FRIEND) robotic arm. In: *AIAA Infotech@Aerospace Conference and AIAA Unmanned...Unlimited Conference*. p. 1870.
- Dupuis E (2001) *A general framework for the manual teleoperation of kinematically redundant space-based manipulators*. PhD Thesis, McGill University.
- Elias AJ and Wen JT (2024) IK-Geo: Unified robot inverse kinematics using subproblem decomposition. *arXiv preprint arXiv:2211.05737v3*.
- FANUC (2022) FANUC R-1000iA/120F-7B robot. <https://www.fanucamerica.com/products/robots/series/r-1000ia/r-1000ia-120f-7b-7-axis-robot>. (accessed Dec. 21, 2022).
- Faria C, Ferreira F, Erhagen W, Monteiro S and Bicho E (2018) Position-based kinematics for 7-DoF serial manipulators with global configuration control, joint limit and singularity avoidance. *Mechanism and Machine Theory* 121: 317–334.
- Flacco F, De Luca A and Khatib O (2012) Motion control of redundant robots under joint constraints: Saturation in the null space. In: *2012 IEEE International Conference on Robotics and Automation*. IEEE, pp. 285–292.
- Franka Emika (2022) Franka production 3. <https://www.franka.de/production>. (accessed Dec. 21, 2022).
- Gong M, Li X and Zhang L (2019) Analytical inverse kinematics and self-motion application for 7-DOF redundant manipulator. *IEEE Access* 7: 18662–18674.
- Gottlieb DH (1986) Robots and fibre bundles. *Bull. Soc. Math. Belg* 38: 219–223.
- Hollerbach JM (1985) Optimum kinematic design for a seven degree of freedom manipulator. In: *Robotics research: The second international symposium*. Citeseer, pp. 215–222.
- Hollerbach JM and Suh K (1987) Redundancy resolution of manipulators through torque optimization. *IEEE Journal on Robotics and Automation* 3(4): 308–316.
- Hopf H (1927) Vektorfelder inn-dimensionalen mannigfaltigkeiten. *Mathematische Annalen* 96(1): 225–249.
- Jiang L, Huo X, Liu Y and Liu H (2013) An integrated inverse kinematic approach for the 7-DOF humanoid arm with offset wrist. In: *2013 IEEE International Conference on Robotics and Biomimetics (ROBIO)*. IEEE, pp. 2737–2742.
- Jin M, Liu Q, Wang B and Liu H (2020) An efficient and accurate inverse kinematics for 7-DOF redundant manipulators based on a hybrid of analytical and numerical method. *IEEE Access* 8: 16316–16330.
- Kim H, Miller LM, Al-Refai A, Brand M and Rosen J (2011) Redundancy resolution of a human arm for controlling a seven DOF wearable robotic system. In: *2011 Annual International Conference of the IEEE Engineering in Medicine and Biology Society*. IEEE, pp. 3471–3474.
- Kim H, Miller LM, Byl N, Abrams GM and Rosen J (2012) Redundancy resolution of the human arm and an upper limb exoskeleton. *IEEE Transactions on Biomedical Engineering* 59(6): 1770–1779.
- Kreutz-Delgado K, Long M and Seraji H (1990) Kinematic analysis of 7 DOF anthropomorphic arms. In: *Proceedings., IEEE International Conference on Robotics and Automation*. IEEE, pp. 824–830.
- Kreutz-Delgado K, Long M and Seraji H (1992) Kinematic analysis of 7-DOF manipulators. *The International Journal of Robotics Research* 11(5): 469–481.
- KUKA (2022) LBR iiwa. <https://www.kuka.com/en-us/products/robotics-systems/industrial-robots/lbr-iiwa>. (accessed Oct. 31, 2022).
- Lamperti C, Zanchettin AM and Rocco P (2015) A redundancy resolution method for an anthropomorphic dual-arm manipulator based on a musculoskeletal criterion. In: *2015 IEEE/RSJ International Conference on Intelligent Robots and Systems (IROS)*. IEEE, pp. 1846–1851.
- Lee KK and Buss M (2006) Redundancy resolution with multiple criteria. In: *2006 IEEE/RSJ International Conference on Intelligent Robots and Systems*. IEEE, pp. 598–603.
- Li S, Han K, He P, Li Z, Liu Y and Xiong Y (2022) Human-like redundancy resolution: An integrated inverse kinematics scheme for anthropomorphic manipulators with radial elbow offset. *Advanced Engineering Informatics* 54: 101812.

- Li Z, Roldan JR, Milutinović D and Rosen J (2013) The rotational axis approach for resolving the kinematic redundancy of the human arm in reaching movements. In: *2013 35th Annual International Conference of the IEEE Engineering in Medicine and Biology Society (EMBC)*. IEEE, pp. 2507–2510.
- Liu W, Chen D and Steil J (2017) Analytical inverse kinematics solver for anthropomorphic 7-DOF redundant manipulators with human-like configuration constraints. *Journal of Intelligent & Robotic Systems* 86(1): 63–79.
- Ma B, Xie Z, Jiang Z and Liu H (2021) Precise semi-analytical inverse kinematic solution for 7-DOF offset manipulator with arm angle optimization. *Frontiers of Mechanical Engineering* 16(3): 435–450.
- Marani G, Kim J, Yuh J and Chung WK (2003) Algorithmic singularities avoidance in task-priority based controller for redundant manipulators. In: *Proceedings 2003 IEEE/RSJ International Conference on Intelligent Robots and Systems (IROS 2003)(Cat. No. 03CH37453)*, volume 4. IEEE, pp. 3570–3574.
- McGrath P (2016) An extremely short proof of the hairy ball theorem. *The American Mathematical Monthly* 123(5): 502–503.
- Motiv Space Systems (2022) xLink space-rated modular robotic arm system. <https://motivss.com/products-capabilities/robotics/xlink/>. (accessed Dec. 21, 2022).
- Mukherji R, Ray DA, Stieber M and Lymer J (2001) Special purpose dexterous manipulator (SPDM) advanced control features and development test results. *Proceedings of the 6th International Symposium on Artificial Intelligence, Robotics and Automation in Space (i-SAIRAS)*.
- Nammoto T and Kosuge K (2012) An analytical solution for a redundant manipulator with seven degrees of freedom. *International Journal of Automation and Smart Technology* 2(4): 339–346.
- Naylor M, Atkins E and Roderick S (2007) Visual target recognition and tracking for autonomous manipulation tasks. In: *AIAA Guidance, Navigation and Control Conference and Exhibit*. p. 6323.
- Needham T (1997) *Visual complex analysis*. Oxford University Press.
- O’Neil K and Chen YC (2000) Instability of pseudoinverse acceleration control of redundant mechanisms. In: *Proceedings 2000 ICRA. Millennium Conference. IEEE International Conference on Robotics and Automation. Symposia Proceedings (Cat. No. 00CH37065)*, volume 3. IEEE, pp. 2575–2582.
- Pfurner M (2016) Closed form inverse kinematics solution for a redundant anthropomorphic robot arm. *Computer Aided Geometric Design* 47: 163–171.
- Pieper DL (1969) *The kinematics of manipulators under computer control*. Stanford University.
- Poincaré H (1885) Sur les courbes définies par les équations différentielles. *J. Math. Pures Appl.* 4: 167–244.
- Productive Robots (2023) OB7 collaborative robots. <https://www.productiverobotics.com/ob7-products/>. (accessed Jun. 21, 2023).
- Pryor JWR (2023) *Teleoperation Methods for High-Risk, High-Latency Environments*. PhD Thesis, Johns Hopkins University.
- Rethink Robotics (2015) Baxter overview. https://sdk.rethinkrobotics.com/wiki/Baxter_Overview. (accessed Dec. 21, 2022).
- Rethink Robotics (2022) Sawyer, the high performance collaborative robot. <https://www.rethinkrobotics.com/sawyer>. (accessed Dec. 21, 2022).
- Robotics Research Corporation (2005) Dexterous manipulators and advanced control systems. Technical report, Robotics Research Corporation. URL <http://www.robotics-research.com/RRCTechDoc.PDF>. Accessed Oct. 31, 2022.
- Scott NA and Carignan CR (2008) A line-based obstacle avoidance technique for dexterous manipulator operations. In: *2008 IEEE International Conference on Robotics and Automation*. IEEE, pp. 3353–3358.
- Seraji H (1989) Configuration control of redundant manipulators: Theory and implementation. *IEEE Transactions on Robotics and Automation* 5(4): 472–490.
- Shi X, Guo Y, Chen X, Chen Z and Yang Z (2021) Kinematics and singularity analysis of a 7-DOF redundant manipulator. *Sensors* 21(21): 7257.
- Shimizu M, Yoon WK and Kitagaki K (2007) A practical redundancy resolution for 7 DOF redundant manipulators with joint limits. In: *Proceedings 2007 IEEE International Conference on Robotics and Automation*. IEEE, pp. 4510–4516.
- Sinha A and Chakraborty N (2019) Geometric search-based inverse kinematics of 7-DoF redundant manipulator with multiple joint offsets. In: *2019 International Conference on Robotics and Automation (ICRA)*. IEEE, pp. 5592–5598.
- Stanczyk B and Buss M (2004) Development of a telerobotic system for exploration of hazardous environments. In: *2004 IEEE/RSJ International Conference on Intelligent Robots and Systems (IROS)(IEEE Cat. No. 04CH37566)*, volume 3. IEEE, pp. 2532–2537.
- Stanczyk B, Peer A and Buss M (2006) Development of a high-performance haptic telemanipulation system with dissimilar kinematics. *Advanced robotics* 20(11): 1303–1320.

- Su H, Enayati N, Vantadori L, Spinoglio A, Ferrigno G and De Momi E (2018a) Online human-like redundancy optimization for tele-operated anthropomorphic manipulators. *International Journal of Advanced Robotic Systems* 15(6): 1729881418814695.
- Su H, Sandoval J, Makhdoomi M, Ferrigno G and De Momi E (2018b) Safety-enhanced human-robot interaction control of redundant robot for teleoperated minimally invasive surgery. In: *2018 IEEE International Conference on Robotics and Automation (ICRA)*. IEEE, pp. 6611–6616.
- Su H, Sandoval J, Vieyres P, Poisson G, Ferrigno G and De Momi E (2018c) Safety-enhanced collaborative framework for tele-operated minimally invasive surgery using a 7-dof torque-controlled robot. *International Journal of Control, Automation and Systems* 16: 2915–2923.
- Su H, Yang C, Ferrigno G and De Momi E (2019) Improved human-robot collaborative control of redundant robot for teleoperated minimally invasive surgery. *IEEE Robotics and Automation Letters* 4(2): 1447–1453.
- Swaim PL, Arend JJ, Bevill PJ, Decker RJ, Dunn JC, Read DA, Reiher RE, Richard BJ, Ruta KJ and Teplitz S (1994) Use of manipulators in assembly of space station freedom. In: Skaar SB (ed.) *Teleoperation and robotics in space, Progress in Astronautics and Aeronautics*, volume 161, chapter 16. Washington, DC: American Institute of Aeronautics and Astronautics, Inc., pp. 443–473.
- Tian X, Xu Q and Zhan Q (2021) An analytical inverse kinematics solution with joint limits avoidance of 7-DOF anthropomorphic manipulators without offset. *Journal of the Franklin Institute* 358(2): 1252–1272.
- Tondu B (2006) A closed-form inverse kinematic modelling of a 7R anthropomorphic upper limb based on a joint parametrization. In: *2006 6th IEEE-RAS International Conference on Humanoid Robots*. IEEE, pp. 390–397.
- Tsumaki Y, Fiorini P, Chalfant G and Seraji H (2001) A numerical SC approach for a teleoperated 7-DOF manipulator. In: *Proceedings 2001 ICRA. IEEE International Conference on Robotics and Automation (Cat. No. 01CH37164)*, volume 1. IEEE, pp. 1039–1044.
- Ufactory (2022) Ufactory xArm 7. <https://www.ufactory.cc/product-page/ufactory-xarm-7>. (accessed Dec. 21, 2022).
- Universal Robots (2022) UR5 collaborative robot arm. <https://www.universal-robots.com/products/ur5-robot/>. (accessed Oct. 31, 2022).
- Wang C, Peng L, Hou ZG, Li J, Luo L, Chen S and Wang W (2019) Kinematic redundancy analysis during goal-directed motion for trajectory planning of an upper-limb exoskeleton robot. In: *2019 41st Annual International Conference of the IEEE Engineering in Medicine and Biology Society (EMBC)*. IEEE, pp. 5251–5255.
- Wang Y and Artemiadis P (2013) Closed-form inverse kinematic solution for anthropomorphic motion in redundant robot arms. *Advances in Robotics and Automation* 2(3).
- Wang Y, Zhao C, Wang X, Zhang P, Li P and Liu H (2021) Inverse kinematics of a 7-DOF spraying robot with 4R 3-DOF non-spherical wrist. *Journal of Intelligent & Robotic Systems* 101(4): 1–17.
- Wang Z and Kazerounian K (1995) Identification and resolution of structural and algorithmic singularity in redundancy control of serial manipulations. *Journal of robotic systems* 12(7): 465–478.
- Xiong G, Zhou Y and Yao J (2020) Null-space impedance control of 7-degree-of-freedom redundant manipulators based on the arm angles. *International Journal of Advanced Robotic Systems* 17(3): 1729881420925297.
- Xu W, She Y and Xu Y (2014) Analytical and semi-analytical inverse kinematics of SSRMS-type manipulators with single joint locked failure. *Acta Astronautica* 105(1): 201–217.
- Yan L, Mu Z and Xu W (2014) Analytical inverse kinematics of a class of redundant manipulator based on dual arm-angle parameterization. In: *2014 IEEE International Conference on Systems, Man, and Cybernetics (SMC)*. IEEE, pp. 3744–3749.
- Yaskawa (2022a) Motoman SIA50D 7-axis robot arm. <https://www.motoman.com/en-us/products/robots/industrial/assembly-handling/sia-series/sia50d>. (accessed Dec. 21, 2022).
- Yaskawa (2022b) Motoman SIA5D 7-axis robot arm. <https://www.motoman.com/en-us/products/robots/industrial/assembly-handling/sia-series/sia5d>. (accessed Dec. 21, 2022).
- Zhao J, Yang X, Zhao Z, Yang G and Zhao L (2023) Inverse kinematics and multi-objective configuration optimization of the SSRMS manipulator. *Advances in Space Research* .
- Zhu X, Wang X and Ma Y (2021) Design and development of teleoperation interactive system for 7-dof space redundant manipulator. In: *2021 5th International Conference on Automation, Control and Robots (ICACR)*. IEEE, pp. 179–183.

Appendix. Index to multimedia extensions

Multimedia extensions are available at <https://www.youtube.com/@AlexEliasRobotics>.

Table of Multimedia Extensions

Extension	Media Type	Description
1	Video	Comparing conventional and stereographic SEW angles
2	Video	Sawyer inverse kinematics solutions using 1D search